Effect of tree demography and flexible root water uptake for modeling the carbon and water cycles of Amazonia

Emilie Joetzjer, Fabienne Maignan, Jérôme Chave, Daniel S Goll, Ben Poulter, Jonathan Barichivich, Isabelle Maréchaux, Sebastiaan Luyssaert, Matthieu Guimberteau, Kim Naudts, et al.

Effect of tree demography and flexible root water uptake for modeling the carbon and water cycles of Amazonia

Emilie Joetzjer[1,2], Fabienne Maignan[1], Jérôme Chave[2], Daniel Goll[1], Ben Poulter[3], Jonathan
5 Barichivich[1,4], Isabelle Maréchaux[2,5], Sebastiaan Luyssaert[6], Matthieu Guimberteau[1,7], Kim
Naudts[6], Damien Bonal[9], Philippe Ciais[1]

[1]Laboratoire des Sciences du Climat et de l'Environnement, LSCE-IPSL (CEA-CNRS-UVSQ), 91190 Gif-sur-Yvette, France
10 [2]Laboratoire Evolution et Diversité Biologique, UMR 5174, Université Paul Sabatier, CNRS, IRD, 31400 Toulouse, France
[3] NASA Goddard Space Flight Center, Biospheric Sciences Laboratory, Greenbelt, MD, USA
[4] Instituto de Conservación, Biodiversidad y Territorio, Universidad Austral de Chile, Valdivia, Chile, and Center for Climate and Resilience Research, Santiago, Chile
15 [5] AMAP, Univ Montpellier, INRA, IRD, CIRAD, CNRS, 34000 Montpellier, France
[6] Vrije Universiteit Amsterdam, Faculty of Science, 1081 HV, The Netherlands.
[7]UMR 7619 METIS, Sorbonne Universités, UPMC, CNRS, EPHE, 4 place Jussieu, 75005 Paris, France
[8] Max Planck Institute for Meteorology, Bundesstraβe. 53, 20146 Hamburg, Germany
20 [9] Université de Lorraine, AgroParisTech, INRA, UMR Silva, 54000 Nancy, France

Correspondence to: emilie.joetzjer@meteo.fr

Abstract.

Amazonian forest plays a crucial role in regulating the carbon and water cycles in the global
25 climate system. However, the representation of biogeochemical fluxes and forest structure in dynamic global vegetation models (DGVMs) remains challenging. This situation has considerable implications to simulate the state and dynamics of Amazonian forest. This study aims at simulating the dynamic of the evapotranspiration (ET), productivity (GPP), biomass (AGB) and forest structure of wet tropical forests in the Amazon basin using the updated ORCHIDEE land
30 surface model. The latter is improved for two processes: stand structure and demography, and plant water uptake by roots. Stand structure is simulated by adapting the CAN version of ORCHIDEE, originally developed for temperate forests. Here, we account for the permanent recruitment of young individual trees, the distribution of stand level growth into 20 different cohorts of variable diameter classes, and mortality due to asymmetric competition for light. Plant water uptake is simulated by
35 including soil-to-root hydraulic resistance (RS). To evaluate the effect of the soil resistance alone, we performed factorial simulations with demography only (CAN) and both demography and resistance (CAN-RS). AGB, ET and GPP outputs of CAN-RS are also compared with the standard version of ORCHIDEE (TRUNK) for which eco-hydrological parameters were tuned globally to fit GPP and evapotranspiration at flux tower sites. All the model versions are benchmarked against in situ and
40 regional datasets. We show that CAN-RS correctly reproduce stand level structural variables (as CAN) like diameter classes and tree densities when validated using in-situ data. Besides offering the key advantage to simulate forest's structure, it also correctly simulates ET and GPP and improves fluxes spatial patterns when compared to TRUNK. With the new formulation of soil water uptake, which is

driven by soil water availability rather than root-biomass, the simulated trees preferentially use water in the deepest soil layers during the dry seasons. This improves the seasonality of ET and GPP compared to CAN, especially on clay soils for which the soil moisture potential drops rapidly in the dry season. Nevertheless, since demography parameters in CAN-RS are constant for all evergreen tropical forests, spatial variability of AGB and basal area across the Amazon remains too uniform compared to observations, and are very comparable to the TRUNK. Additional processes such as climate driven mortality and phosphorus limitation on growth leading to the prevalence of species with different functional traits across the Amazon need to be included in the future development of this model.

1 Introduction

Even though the Amazonian rainforest is of an essential importance for the carbon cycle [*Eltahir and Bras*, 1994; *Werth and Avissar*, 2002] large uncertainties impede future projections of changes in net carbon uptake over Amazonia [*Poulter et al.*, 2010; *Arora et al.*, 2013; *Jones et al.*, 2013]. An analysis of variance on simulation outputs from 12 Earth System models (ESM) showed that uncertainties in projections of terrestrial carbon uptake are primarily driven by model structure [*Lovenduski and Bonan*, 2017]. These uncertainties arise from both the climate projections, especially rainfall [*Ahlström et al.*, 2012] and simulations of the land carbon cycle processes [*Booth et al.*, 2012; *Sitch et al.*, 2015].

In land surface models, sources of uncertainty include the vegetation response to droughts [*Restrepo-Coupe et al.*, 2016], and tree demographic processes [*Fisher et al.*, 2010; *Rödig et al.*, 2018]. Most models simulate the effect of water limitation on plant functioning by lowering leaf gas exchange rates using a stress factor [*Christoffersen et al.*, 2014] and by including atmospheric water stress from high vapor pressure deficit in their parameterization of stomatal conductance. Models typically fail to capture tropical carbon and water flux seasonality [*Poulter et al.*, 2009; *Restrepo-Coupe et al.*, 2016], and the response to drought [*Powell et al.*, 2013; *Joetzjer et al.*, 2014]. A few regional ecosystem models [*Bonan et al.*, 2014; *Christoffersen et al.*, 2016; *Xu et al.*, 2016] and one DGVM [*Kennedy et al.*, 2019] recently adopted a more explicit representation of the soil-plant-atmosphere water column by including formulations of soil-to-root and plant xylem resistances to water transfer.

In the Amazon forest, water uptake is sustained during the dry season, and some forests were even recorded to increase their evapotranspiration and canopy photosynthesis rate in the dry season [*Paca et al.*, 2019], thanks to deep-root water uptake (Maeda et al., 2017). In most global land surface models, water available for transpiration in the root zone is quantified using a root biomass-weighted sum of moisture in different soil layers, with a decreasing root biomass profile at depth. Under this assumption, the upper soil layers with higher root biomass contribute more to soil water uptake, which may lead to an overestimation of the water stress when those layers dry out. In the reality, the soil-to-root water flow depends on soil and root hydraulic properties, which vary in time and with depth [*Sperry et al.*, 2002]. Tree water potentials were observed to preferentially equilibrate with the wettest part of the soil [*Schmidhalter*, 1997], a process controlled not only by the density of roots but also by the

variability of both the soil-to-root resistance and the root activity within the soil profile. In turn, the soil-to-root resistance is non-linearly related to soil water content [*Gardner*, 1960]. In this study, we introduced a new root water uptake scheme that includes a soil-to-root resistance, in the soil hydrology module of the ORCHIDEE model and tested it over the Amazon for evapotranspiration (ET (mm d^{-1}) or LE (W m^{-2})) and photosynthesis (gross primary productivity, GPP), as well as above ground biomass (AGB).

Most current global land surface models simulate forest wood biomass as a single pool of carbon that receives input from the fraction of primary productivity allocated to wood and losses carbon from mortality. Mortality is often assumed to be a fixed fraction of biomass, but some models include a climate-dependent mortality, based e.g. on empirical relations. Photosynthesis is usually simulated using a big-leaf approximation. In the reality, field observations have highlighted the importance of competition between individuals leading to stand structure and demography [*Farrior et al.*, 2016], which control stand level height, biomass and productivity of tropical forests [*Johnson et al.*, 2016a]. Forest stand models have been developed to include competition-dependent growth and mortality [e.g. *Sakschewski et al.*, 2016; *Maréchaux and Chave*, 2017; *Longo et al.*, 2018]. They explicitly represent forest dynamics via tree demography and vertical competition for light. In some models, forest structure and tree demography emerge from a mechanistic representation of competition and recruitment schemes with different individuals or species or groups of species having various functional traits. Differentiation between traits in a stand model can bring insights on forests resilience [*Zhang et al.*, 2015; *Levine et al.*, 2016; *Sakschewski et al.*, 2016; *Xu et al.*, 2016; *Fisher et al.*, 2018; *Longo et al.*, 2018].

At face value, stand models have complex parameterizations and require multiple drivers that make them difficult to run at large scale. They also generally lack detailed soil hydrology and energy budget calculations, as implemented in land surface models. In this study, we adapt an intermediate complexity approach to simulate stand structure in the land surface model ORCHIDEE, based on the representation of different tree cohorts among which stand-level simulated growth is distributed and mortality is calculated from the density of trees, using self-thinning principles. This approach pioneered by *Bellassen et al.*, [2010, 2011] was further developed in the CAN version of ORCHIDEE by *Naudts et al.*, [2015] for temperate and boreal forests. Here we extend it to tropical rainforests by adding recruitment of young trees following gap formation, by revisiting the self-thinning law, that is observed to be an emerging property of tropical stands [*Pillet et al.*, 2017].

To improve wet tropical forest over the Amazon structure and seasonal fluxes dynamic simulation, we propose an improved version of the ORCHIDEE land surface model. ORCHIDEE is improved for two processes: (1) stand structure and demography, and (2) plant water uptake by roots including a soil-to-root water resistance. This study aims at simulating the water, and carbon (GPP) fluxes, biomass (AGB) and forest's structure of wet tropical forests over the Amazon. Both processes were incorporated in the ORCHIDEE-CAN-RS model code here-after being called CAN-RS. The differences in simulation output between CAN-RS and CAN allow us to evaluate the effect of soil-root (RS) hydraulic processes. The

3

differences between CAN-RS, CAN and the standard version of ORCHIDEE, called TRUNK, allow us to evaluate the effect of forest demography. We used the TRUNK version updated for the CMIP6 exercise (Peylin et al., in prep). Data used for evaluation over the Amazon include eddy-covariance measurements of GPP and ET (LE) as well as soil moisture, site-level forest inventory data for biomass, density and stand structure, and gridded GPP and ET products from observation-based models across the entire basin.

2. Methods

2.1 Model description and experimental design

2.1.1 Transpiration and biomass dynamics in TRUNK, CAN and CAN-RS

The ORCHIDEE land surface model first described by *Krinner et al.,* [2005] represents energy, water, and carbon exchanges within the soil-plant-atmosphere continuum on a half-hourly time step. In the TRUNK version, carbon assimilation is based on the leaf-scale equation of *Farquhar et al.*, [1980] for C3 plants and the stomatal conductance formulation of Yin and Struijk (2009), with an analytical equation to compute assimilation and stomatal conductance (g_S) at each time-step. Evapotranspiration is the sum of evaporation from bare soil, evaporation of water intercepted by the canopy, and transpiration. Transpiration is controlled by g_S and by the evaporative demand of potential evapotranspiration. Stomatal conductance is reduced by atmospheric water stress with a decreasing function of vapor pressure deficit (VPD) and by soil-moisture water stress using an empirical function of the root biomass-weighted soil moisture [*de Rosnay and Polcher*, 1998] (see SI section D).

In the CAN version [*Naudts et al.*, 2015; *McGrath et al.*, 2016] the big-leaf approach was replaced by a dynamic three-dimensional representation of the canopy based on *Haverd et al.*, [2012]. Carbon assimilation and leaf transpiration are scaled from each leaf layer to the canopy based on light intercepted by leaf area (leaf area index, LAI) layers, with an exponential attenuation of light from the top of the canopy to the ground. The soil moisture stress function differs from the TRUNK. The constrain on transpiration is based on the amount of water plants can transport from the soil to their leaves. If the transpiration rate exceeds the plant water supply, the stomatal conductance is reduced until equilibrium is reached. This approach accounts for the total hydraulic resistance of the water transport from roots to leaves, through the sapwood xylem flow, described by *Hickler et al.*, [2006] and *Naudts et al.*, [2015]. Both CAN and TRUNK have the same 12-layer soil diffusion model [*Guimberteau et al.*, 2014]. Changes made to the root water uptake formulation with the inclusion of a new soil-to-root resistance formulation in CAN-RS are described in section 2.1.3

In TRUNK the dynamics of woody biomass is modelled as a single pool with constant loss due to mortality and a weather-dependent input from the fraction of NPP allocated to woody tissues. The model distinguishes sapwood and heartwood to compute tree woody respiration, with a constant fraction of sapwood becoming heartwood at each time step. In CAN, forest biomass is calculated with tree demography, which is simulated by distributing stand-level net

primary productivity (NPP) to a user-defined number of tree diameter classes (20 classes) following the diameter-dependent allocation rule of *Deleuze et al.*, [2004], as originally implemented by *Bellassen et al.*, [2010]. This rule gives more NPP to the largest diameter classes, thus demoting smaller trees. Mortality due to the competition between diameter classes is based on an empirical relationship between biomass and diameter known as self-thinning [*Reineke*, 1933]. There is good evidence for self-thinning in -aged temperate and boreal forests in the literature, but less so for wet tropical forests. Here, we assumed that self-thinning can be applied over Amazon tropical forests, based on data from [*Kohyama*, 1992; *Phillips et al.*, 2002; *Pillet et al.*, 2017] that show a decrease of the logarithm of stand tree density as a function of the logarithm of mean tree diameters, although with site-specific slopes and larger noise than in temperate and boreal stands. Because CAN was originally parameterized and evaluated for temperate an boreal latitude forests [*Naudts et al.*, 2015], we recalibrated the self-thinning equation (based on [*Yoda et al., 1963*])and added the recruitment of young trees, which is a key process controlling the demography and biomass of tropical forests. These changes are described below in section 2.1.2, and evaluated in the manuscript (section 3.4). Additional parameter values adjustments are listed in the Supplementary Information.

2.1.2 Self-thinning and recruitment (CAN and CAN-RS)

In CAN, the competition for light among tree diameter classes is based on the self-thinning equation that relates the maximum number of trees (N_{max}) to the mean stand diameter D_g (m)

$$N_{max} = \left(\frac{D_g}{\alpha}\right)^{1/\beta} \tag{1}$$

The parameters $\alpha = 1100$ (m) and $\beta = -0.57$ were estimated for tropical forests using publicly available plot-level data from the RAINFOR forest inventory network [*Brienen et al.*, 2015]. This tropical self-thinning relationship is represented in Fig 1a.

In unmanaged tropical forests, the recruitment of small trees is fostered by gap creation due to the death of large trees which locally increases light availability [Denslow et al., 1998]. While gaps are not explicitly represented in CAN, to account for this natural forest regeneration, we implemented a recruitment scheme where the number of recruited new trees ($N_{recruits}$ per hectare and per year, Fig. 1b) is a function of the LAI of the remaining trees using the following equation:

$$N_{recruits} = 100exp(-0.15LAI) \tag{2}$$

This parameterization assumes, following Ruger et al., (2009) that the number of recruits depends on mean-stand LAI because a higher LAI will reduce light availability in the understory and hence hinder sapling recruitment and growth. The order of magnitude of the computed number of recruited trees is comparable to those observed in Amazonia [*Phillips and Gentry*, 1994; *Lewis et al.*, 2004, *Phillips et al., 2004*]. The effects of the inclusion of

215 recruitment on forest structure and carbons fluxes are detailed in the Supplementary
Information (section B2). The recruitment formulation is illustrated in Fig. 1b.
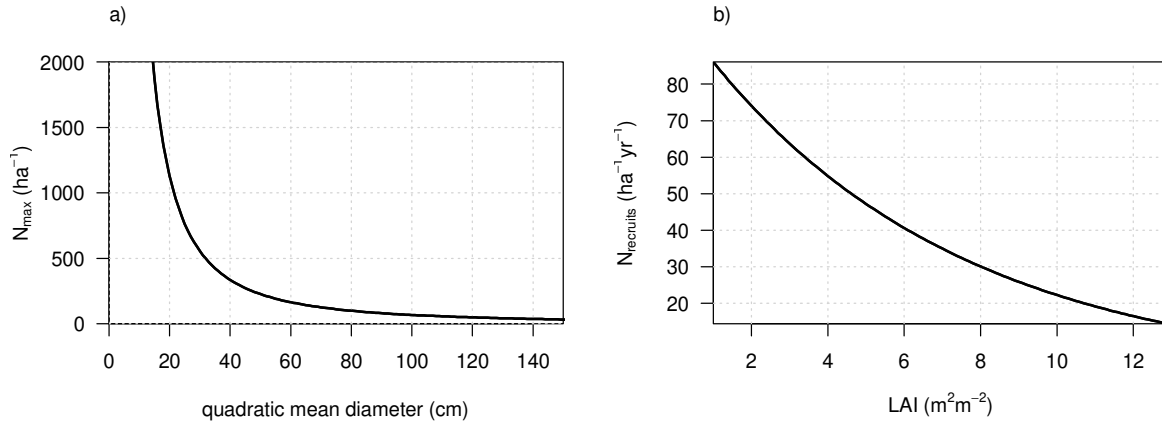
Figure 1. (a) Self-thinning relationship (equation 1) and (b) recruitment function of new trees (equation 2) implemented in this study

220

2.1.3 Dynamic root water uptake with variable soil-to-root resistance (CAN-RS)

In CAN, the soil water potential in the rooting zone (Ψ_{rz}, MPa) is calculated as the sum of the soil water potentials per layer (Ψ_s, MPa) weighted by the relative proportion of root biomass
225 in each layer (d_{root}), with a fixed root biomass profile that decreases exponentially with depth. Processes controlling the water transfer from soil to roots, which are not explicitly represented, are accounted for by adding a tuning factor (m_ψ) to the modeled soil water potential to simulate the root zone water potential [*Naudts et al.*, 2015] :

230 $$\Psi_{rz} = \sum_{l=1}^{L}[\Psi_s(l)d_{root}(l)] + m_\psi \tag{3}$$

where *L* is the number of layers (*L*=12) and *l* the index of the considered layer.

Ψ_s is calculated for each soil layer *l* as a function on the simulated volumetric water content of
235 that layer ($SWC(l)$,m^3 m^{-3}) following the Mualem - van Genuchten model [*Mualem*, 1976; *van Genuchten*, 1980]:

$$\Psi_s(l) = max\left(\frac{1}{k_{av}}\left(\left(\frac{SWC(l)-\Theta_r}{\Theta_r-\Theta_s}\right)^{\frac{-1}{k_{nv}}} - 1\right)^{\frac{1}{k_{nv}}} ; -5\right) \tag{4}$$

240 where *SWC(l)* is the relative soil water content in layer *l*; Θ_r and Θ_s (m^3 m^{-3}) are the residual and saturated soil water contents, respectively; and k_{av}, k_{nv} are the van Genuchten parameters. These parameters are soil texture-dependent (see Table S1). Ψ_s cannot be lower than a minimum soil water potential for hygroscopic water of -5 MPa [*Larcher*, 2003].

6

245   The use of root biomass-weighted soil water potentials in the soil profile in Eq. (3) ignores the dependence of soil-to-root water flow on soil and roots hydraulic properties. Besides, the fixed value of the m_ψ tuning parameter may lead to incorrect positive hydraulic potentials in the soil. We implemented in this study a different computation of Ψ_{rz}, whereby Ψ_s is weighted by $E_{max}(l)$ (mmol m^2 s^{-1}), the maximum amount of water that can be absorbed by
250   the roots in each layer, which itself depends on the soil-to-root resistance R_{sr} (MPa s mmol^{-1} m^{-2}) and on a minimum root water potential $\Psi_{root,m}$ (MPa) [*Williams et al.*, 2001; *Fisher et al.*, 2006; *Duursma and Medlyn*, 2012]. This is given by replacing Eq. (3) by the following equation:

255   $\Psi_{rz} = \frac{\sum_1^L \Psi_s(l)E_{max}(l)}{\sum_1^L E_{max}(l)}$ with $E_{max}(l) = [\Psi| \quad |s(l) - \Psi_{root,m}]/R_{sr}(l)$

                                                    (5)

The minimum root water potential $\Psi_{root,m}$ is set at -3 MPa [*Duursma and Medlyn*, 2012]. The soil-to-root resistance R_{sr} estimates the effective path length for water transport from the soil
260   matrix to the root surface [*Gardner*, 1960], and is computed as follows:

$R_{sr}(l) = \frac{ln\left(\frac{r_s(l)}{r_r}\right)}{2\pi l_r(l)G_{soil}(l)\Delta_D(l)}$ (6)

where l_r (m^{-2}) is the root length per unit of soil volume, a function of the specific root length
265   (*SRL*), here set at 10 m g^{-1} [*Metcalfe et al.*, 2008]. l_r also depends on the fine root biomass density per layer ($Biomass_{froots}(l)$, in g m^{-3}) and is calculated as follow $l_r(l) = Biomass_{froots}(l)SRL$. r_s (m) is one-half of the mean distance between roots, computed following [*Newman*, 1969]:

270 $r_s = \left(\frac{1}{\pi l_r(l)}\right)^{0.5}$ (7)

In equation (6), r_r (m) is the mean fine root radius, set at 0.29 10^{-3} m [*Bonan et al.*, 2014]; G_{soil} (mmol m^{-1} s^{-1} MPa^{-1}) is the soil saturated hydraulic conductivity. $Biomass_{froots}$ represents the sum of fine root biomass of all the cohorts calculated following the allocation
275   scheme relying on the pipe model theory as implemented originally in CAN [*Shinozaki*, 1964; *Sitch et al.*, 2003] and it is vertically discretized per soil layer by multiplying by $d_{root}(l)$. $\Delta_D(l)$ (m) represents the thickness of the soil layer l.

2.1.4 Soil hydraulic parameters defining texture-dependent soil water potentials

280   In all three versions of ORCHIDEE considered in this study, the relationships between saturated hydraulic conductivity (G_{soil}), volumetric water content (SWC), and soil water potential (Ψ_s) are described by the Mualem–van Genuchten model [*Mualem*, 1976; *van Genuchten*, 1980], using the parameters estimated by *Carsel and Parrish*, [1988] for the 12 soil texture classes of the United States Department of Agriculture (USDA) classification.

285 TRUNK has been calibrated and evaluated at global scale and specifically over Amazonia [*Getirana et al.*, 2014; *Guimberteau et al.*, 2014] using this USDA parameterization. To ensure consistency between the different model versions compared in this study, and model's development traceability, we used the same parameter values to define soil water potential as a function of soil moisture in each layer (equation 4; parameter values are given in Table S1).

290 .
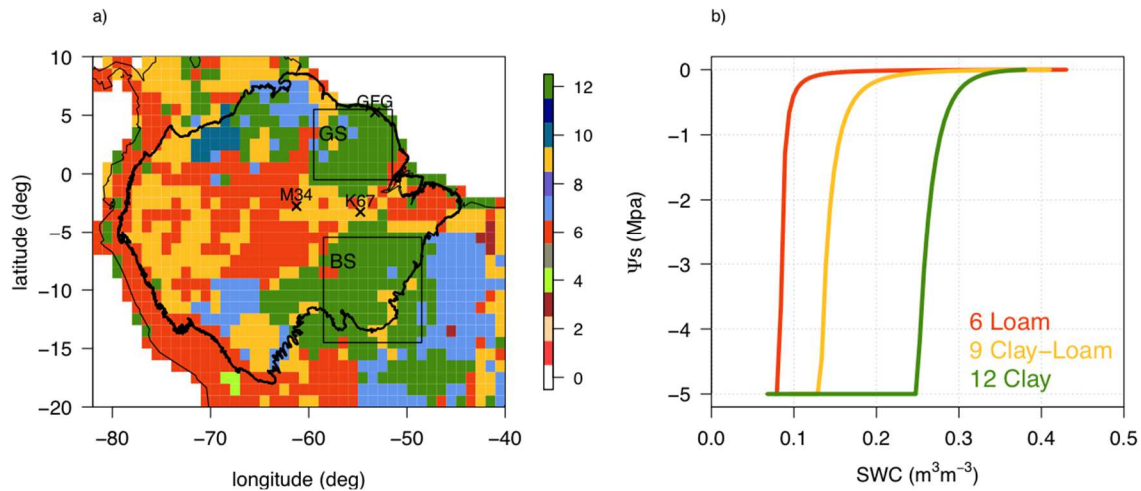
Figure 2. (a) USDA soil types interpolated at 1-degree resolution over the Amazon. The regions in the black squares denoted GS and BS are part of the Guiana and Brazilian Shields where the model was evaluated; (b) soil water retention curves defining the soil
295 **water potential Ψ_s versus the volumetric water content SWC predicted by the Mualem-van Genuchten equation (Eq. 4) for the three dominant soil classes in Amazonia.**

The spatial heterogeneity of soil structure in Amazonia is related to the geology of the area with old, highly weathered soils (Precambrian substrates) over the Brazilian and Guiana
300 Shields contrasting with much younger Cenozoic soils of the Andes and western Amazonia [*Quesada et al.*, 2011]. This is reflected in the USDA map of soil types, with mainly clay (12) over the shields, and loam (6) and clay-loam (9) over the rest of Amazonia (Fig. 2a). The Mualem-van Genuchten equation (Eq. 4) implies a lower water availability for plants in clay soils than in loamy or clay-loamy soils, at a given soil water content, that is, more negative
305 values of Ψ_s for the same SWC, as shown in Fig. 2b.

2.1.5 Simulations

We compared outputs from the TRUNK version used in the 6th Model Intercomparison Project (CMIP6), from CAN (v2290) with self-thinning, recruitment and parameters modified
310 for tropical forests as presented in section 2.1.2, and from CAN-RS which additionally includes the new root water uptake module. Note that even though, ORCHIDEE-CAN simulates forest structures, it does not yet include species co-existence and competition between species. ORCHIDEE is a global land surface model that describes vegetation using a gridded classification of land cover represented by 13 plant functional type (PFTs) (one for
315 bare soil, eight for forests, two for grasslands and two for croplands), each characterized by a specific set of parameters. Most of the Amazon forest is represented by the evergreen tropical forest plant functional type (Fig. 12a), with the multi-layer soil water diffusion scheme [*de*

Rosnay et al., 2002] parameters given in section 2.1.4 and a 4-meter uniform soil depth [*Campoy et al.*, 2013].

320

Site level simulations were performed for three tropical evergreen forests for which eddy-covariance measurements were available (da Rocha, 2004): Santarem KM67 (K67), Manaus KM34 (M34) [*da Rocha et al.*, 2009] and Paracou (GFG) [*Bonal et al.*, 2008]. All simulations used hourly local meteorological forcing. Each site corresponds to one of the major soil
325 texture classes of the USDA soil classification (Fig. 2 and Table 1). Secondly, historical simulations were performed at 1-degree spatial resolution over the Amazonian forest using gridded climate forcing data from CRU-NCEP, which combine monthly data from the Climate Research Unit (CRU) and 6-hourly fields from the National Center for Environmental Prediction (NCEP) [*Wei et al.*, 2014] (Table 1). All simulations started from a
330 semi-analytical spin-up [*Lardy et al.*, 2011] to equilibrate carbon and hydrological variables by recycling climate data from 1981 to 2000 under a constant CO_2 concentration set to 350 ppm.

Table 1. Summary of the simulations performed with the three versions of ORCHIDEE.

	Simulation name	Soil type	USDA	Meteorological data	Period
local	K67	clay-loam	9	In situ meteorological measurements (hourly)	2002-2004
	M34	loam	6		2003-2005
	GFG	clay	12		2007-2009
regional	REGIONAL	USDA texture maps (Fig. 2)		CRU-NCEPv7.1 (6 hourly)	1981-2016

335

2.2 Evaluation data

2.2.1 Site data

At all three flux tower sites, we used eddy-covariance measurements of hourly sensible (H) and latent (LE) heat fluxes, and net ecosystem carbon exchange (NEE). LE (W m^{-2}) is
340 equivalent to the evapotranspiration (mm d^{-1}) [*Bonal et al.*, 2008; *da Rocha et al.*, 2009]. To convert LE in ET, LE is multiplied by the latent heat of vaporization (λ) that is a factor depending on air temperature. Gross primary productivity (GPP) and ecosystem respiration were separated from NEE using the algorithm of *Reichstein et al.*, [2005].. Flux data are noisy, and *Hollinger and Richardson*, [2005] evaluated the relative uncertainty of H, LE and
345 CO_2 fluxes derived from eddy-covariance measurements to be around 25% for a temperate forest. For eddy-covariance data, energy balance closure is a good proxy for data quality [*Wilson*, 2002]. We therefore calculated the overall energy balance ratio as the ratio of the sum of outgoing radiation (LE + H) divided by the sum of incoming radiation averaged over the study period [*Wilson*, 2002] (Table. 1). K67 and GFG showed a good energy closure (ratio
350 of 1.008 and 0.96 respectively), but at M34 this ratio was only of 0.69, suggesting that LE or/and H are underestimated.

Field observations of LAI, basal area (BA), and canopy height (Table 2), were used to evaluate the models at each site. At K67, vertical soil moisture measurements [*Nepstad et al.*, 2007] were used to test the soil water temporal dynamics in the CAN-RS version. At GFG, old-growth forest plots were surveyed [*Gourlet-Fleury et al.*, 2004; *Ho Tong Minh et al.*, 2016]. We used tree diameter and height measurements (for 1592 trees) from the 2014 inventory on a 6.25 ha plot in order to evaluate CAN and CAN-RS forest structure representation. Forest inventories used in this study only included trees with a diameter at breast height (DBH) above 10 cm. Statistically time-extended data from a site near to GFG that was clear-cut in 1976 and then left to regenerate were also used to evaluate forest biomass and stand density dynamics in CAN and CAN-RS [*Chave et al., in prep*].

2.2.2 Regional data

To evaluate GPP patterns and seasonality across the Amazon, we used monthly outputs of the observation-based GPP FLUXCOM model ensemble from 1981 to 2013 at a 0.5° resolution, obtained by using different methods to upscale eddy-covariance data by *Tramontana et al.*, [2016] and *Jung et al.*, [2017]. We calculated the median of three FLUXCOM models, namely ANNs (artificial neural networks), RF (Random Forest) and MTE (Model Tree Ensemble) that all used the method proposed by *Lasslop et al.*, [2010] to retrieve GPP by fitting a respiration model to nighttime NEE values. Compared to the global network of flux-tower measurements, the FLUXCOM models performances were reasonable in terms of annual mean and spatial pattern representation ($R^2 > 0.7$) and mean seasonal cycle ($0.67 < R^2 < 0.77$), but the models showed a low predictive power for inter-annual variability ($R^2 = 0.13$) [*Tramontana et al.*, 2016]. Also, GPP was better predicted by FLUXCOM models at temperate sites compared to tropical ones, given the scarcity of tropical sites to train models [Table C3, *Tramontana et al.*, 2016]. For ET, we used the remotely-sensed GLEAM v3.1a product [*Martens et al.*, 2017 and references within] interpolated at a 1° resolution from 1981 to 2016. GLEAMv3.1 was compared to site-level ET measurement at K67 (M34) between 2000 and 2006 by *Moreira et al.*, [2018] who found a relatively strong bias of 0.77 (0.99) mm d^{-1} and low correlation -0.08 (0.32), suggesting that this dataset is uncertain for the Amazon. To evaluate large scale biomass and stand structure, we used the data from 413 ground inventories across Amazonia presented by *Mitchard et al.*, [2014]. Basal area (BA) was directly calculated from diameter measurements, and aboveground biomass (AGB) was calculated at each site using the three-parameter moist tropical forest allometric model of *Chave et al.*, [2005].

3. Results

3.1 Site-level evaluation of the models

3.1.1 Yearly means

CAN and CAN-RS outperform TRUNK to simulate yearly mean of LE at K67 and GFG (Table 2). Note that CAN-RS simulates the annual mean being simulated with a bias of about 3.5%. However at M34, CAN and CAN-RS overestimated LE with a large bias (> 60 %) (Table 2), but we should keep in mind that the energy budget is not closed at this site (see

10

2.2.1). For GPP, TRUNK slightly outperformed CAN and CAN-RS at K67, but CAN and CAN-RS outperformed TRUNK at the two other sites. Note that at GFG, CAN-RS outperformed CAN for both LE and GPP. TRUNK simulated a lower AGB than observed, while CAN and CAN-RS generally overestimated AGB, especially at K67, where the
400 overestimate by CAN and CAN-RS was 25% and 31%, respectively. This overestimation of AGB may possibly result from previous disturbances such as the droughts associated with the strong El Niño events of the 1990s (Pyle et al., 2008) that these simulations forced by 3 years meteorological forcing cannot represent. At the two other sites AGB is better captured by CAN and CAN-RS. Finally, CAN and CAN-RS tended to underestimate tree height and
405 overestimate basal area (Table 2). Height and basal areas are not modeled in TRUNK.

Table 2. Comparison of the three versions of ORCHIDEE against site observations. Mean absolute percentage bias between observations and model results are indicated in italic

VARIABLE	Site	OBS	TRUNK	CAN	CAN-RS	Refs and remarks
LE $(W\ m^{-2})$	K67	86	70 *(18.6)*	87 *(1.2)*	89 *(3.5)*	Eddy-covariance measurements [*Bonal et al.*, 2008; *da Rocha et al.*, 2009]
	M34	79	91 *(15.2)*	132 *(67.1)*	131 *(65.8)*	
	GFG	119	92 *(22.7)*	102 *(14.3)*	115 *(3.4)*	
GPP $(\mu mol\ CO_2\ m^2\ s^{-1})$	K67	8.2	7.7 *(6.1)*	6.3 *(23.2)*	7.4 *(9.8)*	
	M34	7.9	7.5 *(5.1)*	8.1 *(2.5)*	8.1 *(2.5)*	
	GFG	9.7	7.6 *(21.6)*	7.8 *(19.6)*	9.6 *(1.0)*	
AGB $(tC\ ha^{-1})$	K67	148 ± 3	101 *(31.8)*	198 *(33.8)*	214 *(44.6)*	[*Pyle et al.*, 2008] recently disturbed plot [*Malhi et al.*, 2009b] [*Dubois-Fernandez et al.*, 2012]
	M34	180 ± 10	99 *(45.0)*	221 *(22.8)*	221 *(22.8)*	
	GFG	203	102 *(49.8)*	206 *(1.5)*	228 *(12.3)*	
LAI $(m^2\ m^{-2})$	K67	6.4 ± 0.1	4.9 *(23.4)*	6.2 *(3.1)*	6.6 *(3.1)*	[*Malhi et al.*, 2009a]
	M34	5.6 ± 0.2	4.8 *(14.3)*	6.7 *(19.6)*	6.7 *(19.6)*	[*Malhi et al.*, 2009a]
	GFG	8.6 ± 0.7	5.0 *(41.9)*	6.5 *(24.4)*	7.3 *(15.1)*	[*Granier et al., 1996*]
Canopy Height (m)	K67	29.1 ± 7.2	-	19 *(34.7)*	19.1 *(34.4)*	[*Meyer et al.*, 2018] mean canopy height model (CHM) at 1 m resolution from LIDAR and associated standard deviation
	M34	26.7 ± 6.8	-	19.5 *(27.0)*	19.6 *(26.6)*	
	GFG	29.7 ± 9.5	-	19.4 *(34.7)*	20.2 *(32)*	
Basal Area $(m^2\ ha^{-1})$	K67	31	-	36.1 *(16.5)*	36.2 *(16.8)*	[*Hunter et al., 2008*]
	M34	27	-	36.6 *(35.6)*	36.6 *(35.6)*	[*Rodrigues et al., 2001*]
	GFG	31.6	-	36.5 *(15.5)*	37.3 *(18)*	[*Ferry et al., 2006*] (Table 4)

410

3.1.2 Seasonal water and carbon fluxes

Analyzing the time series of LE, GPP and NEE at the three sites through Taylor diagrams [*Taylor*, 2001], the three models performed reasonably well with temporal correlations between observations and simulations varying from 0.5 to 0.8 and the normalized standard
415 deviation and RMSE both going from 0.5 to 1 (Fig. 3). CAN-RS outperformed CAN at K67 and GFG, and both models showed similar performances at M34 (Fig. 3). CAN and CAN-RS did not exhibit systematically better correlations with the data compared to TRUNK, but did have a lower standard deviation.
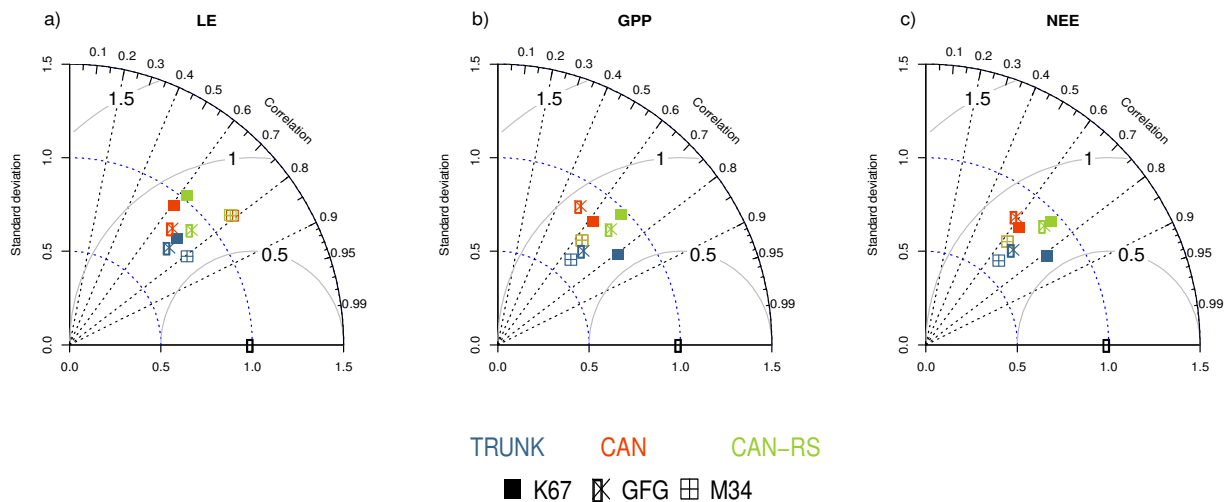
Figure 3. Taylor Diagrams for: (a) LE, (b) GPP and (c) NEE, at three Amazonian sites equipped with an eddy-flux tower system. These quantities were calculated among hourly values removing nighttime values (defined by downwelling shortwave radiation ≤ 5 W m^{-2}). In a Taylor diagram, equal correlation extends radially from the origin. The blue concentric lines indicate identical ratios of standard deviation of the simulated flux to the observed flux. The grey lines represent identical root mean square errors (RMSE) of the centered fluxes.
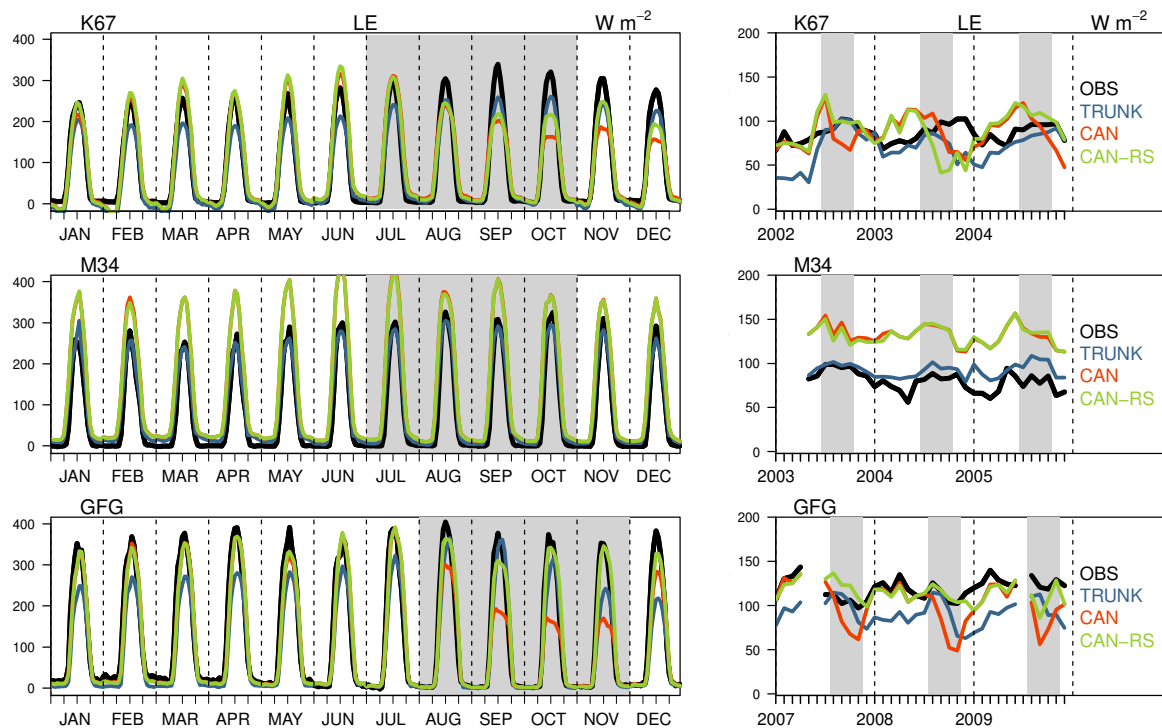
The effect of the soil-to-root resistance scheme on LE and GPP was strongly dependent on the soil type (Table 1 and Fig. 2). Little difference between CAN and CAN-RS was observed at site M34, where the soil is loamy, implying a low water stress most of the year. At site GFG however, soil is clayey implying a higher water stress during the dry season, and CAN-RS performed better than CAN, which underestimated LE and GPP by 31% and 54%, respectively, during the dry season. For site K67 with a clayey-loamy soil, implying an intermediate water stress, CAN-RS buffered the dry season drop in LE and GPP simulated by CAN during the first (2002) and third years (2004). In 2003, CAN-RS simulated a decrease in LE and GPP two months sooner than CAN (Figs. 4 and 5). In summary, we found that CAN-RS and CAN had very similar results during the wet season, but CAN-RS better simulated the seasonality of LE and GPP than CAN for soils prone to water stress during the dry season. This is because the new root water uptake module alleviated drought stress by allowing a shift in water uptake from drier superficial layers to wetter deeper soil layers. On the other hand, CAN-RS and CAN simulated a midday depression for GPP during dry seasons, which is not apparent in the data, resulting in a lower hourly correlation between observations and simulations than for the TRUNK version (Fig. 5).
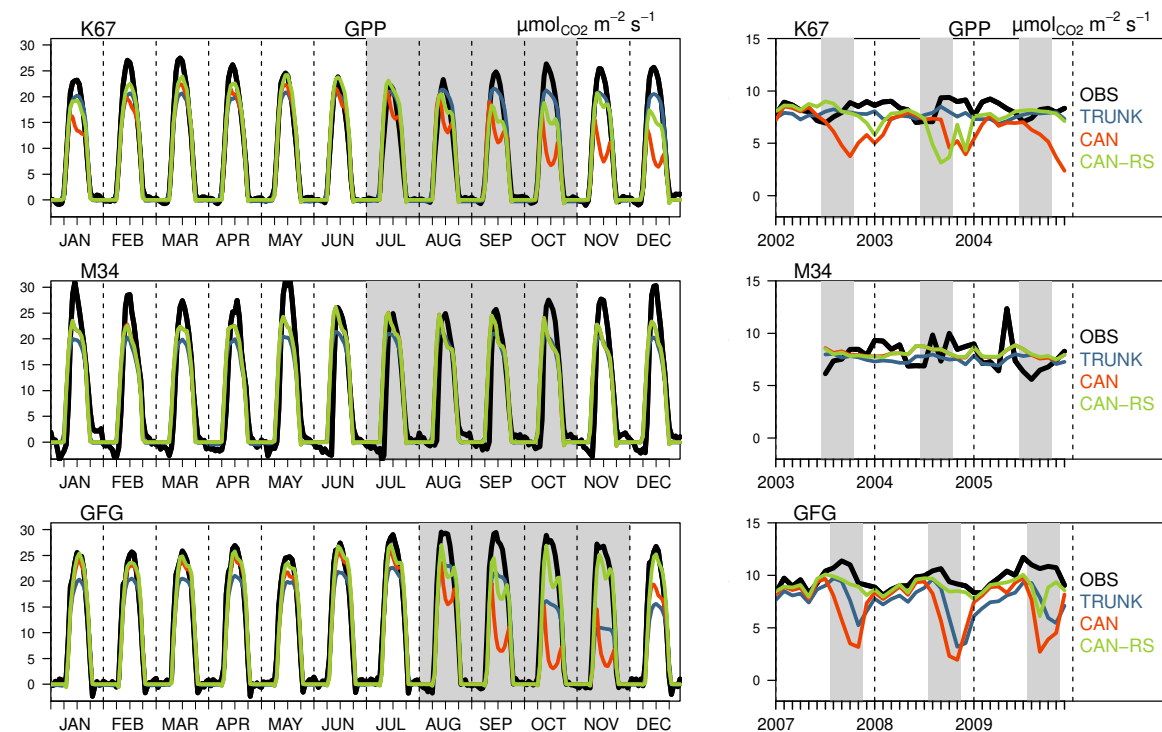
Figure 4. Observed and simulated LE (W m⁻²) at the three sites. Left panels show the average diurnal cycle for each month over three years; and right panels, monthly mean time series. Grey shaded areas indicate dry seasons (here defined as periods with precipitation less than 100 mm per month).

Figure 5. Observed and simulated GPP (μmolCO₂ m⁻² s⁻¹) at the three sites. Left panels show the average composite monthly diurnal cycle for each month over 3 years; and right panels, monthly mean time series. Grey shaded areas indicate dry seasons (here defined as periods with precipitation less than 100 mm per month).

13

3.1.3 Soil volumetric water content and transpiration

460 To better understand the effect of the new root water uptake scheme, we focus here on the K67 site, where the soil water content was measured at different depths. Deviations between observations and simulations may be due to using soil texture and van Genuchten parameters from the USDA soil parameterization : these may be different from actual soil at K67 (Figs. 6b-d). Besides, soil water content tended to be lower in CAN-RS than in CAN, especially

465 during the dry seasons, in agreement with the higher LE simulated by CAN-RS (Fig. 4).
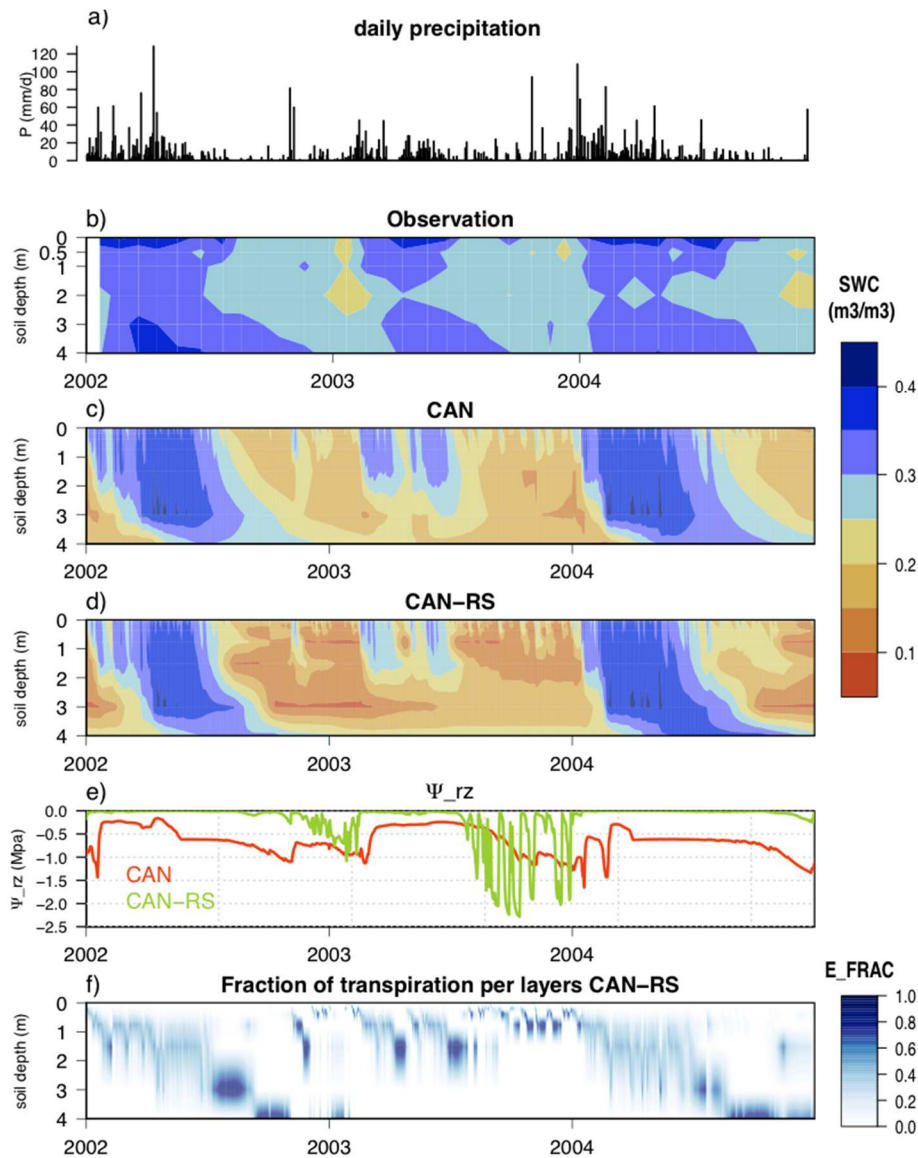
Figure 6. Daily times series from 2002 to 2004 at K67 of (a) precipitation, (b) observed soil moisture profile, (c) soil moisture (SWC) profile simulated in CAN (d) and soil

470 **moisture (SWC) profile simulated in CAN-RS, (e) soil water potential in the rooting zone (Ψ_{rz}), and (f) simulated soil profile of the contribution of each layer to total root water uptake $E_{frac}(l)$ from CAN-RS, defined as $E_{max}(l)$ divided by the sum of E_{max} across all layers.**

14

475 For the years 2002 and 2004, the new root water uptake module allowed CAN-RS to overcome the too strong tree water stress simulated by CAN during dry seasons (see Figs. 4 and 5) and Ψ_{rz} stayed close to zero (Fig. 6e). Wet season rainfall restored soil moisture in all soil layers from top to bottom (Fig. 6d), and most layers then contributed to the transpiration flux (Fig. 6f). As the dry season progressed, the topsoil layers became drier due to stronger

480 evaporation, which induced a shift of water uptake towards deeper and wetter soil layers (Fig. 6f), where the soil-to-root resistance is lower (Eq. 6), and, therefore, E_{max} is higher (Eq. 7). Since the 2003 wet season was drier (1276 mm) than in 2002 (1683 mm) and 2004 (1849 mm) (Fig. 6a), the amount of precipitation was insufficient to recharge the soil after the dry-season depletion in the model (Fig. 6c-d) but not in the observations (Fig. 6b) explaining the

485 mismatch between the observed and simulated fluxes (Fig 4 and 5). This delay in recharging the soil in the wet season may be due to underestimated vertical infiltration (e.g. an underestimation of the current parameters for soil conductivity, ignored preferential drainage/infiltration along plant roots) or to the lack of groundwater storage mechanisms in the model. This translates into strong hydrological stress during the 2003 dry season, with

490 daily Ψ_{rz} reaching -2.3 MPa (Fig. 6e). This failure of the model to completely recharge the soil profile during the wet season of 2003 caused a significant reduction in the simulated LE and GPP in that year (Figs. 4 and 5).

495 **3.1.4 Forest biomass and structure**

We found that CAN and CAN-RS correctly reproduced forest establishment from bare soil based on statistically time-extended empirical data from the site in French Guiana (Chave et al., in prep) where biomass and basal area were measured for 32 years after clear-cut and

500 natural regeneration (Fig. 7), starting with a fast increase in AGB and BA, which levelled off as self-thinning began. The higher AGB simulated by CAN-RS (and CAN) compared to TRUNK is mainly explained by a higher carbon use efficiency, that is a higher ratio of NPP to GPP, which is discussed in section 3.2.2 and shown in Fig. S3.
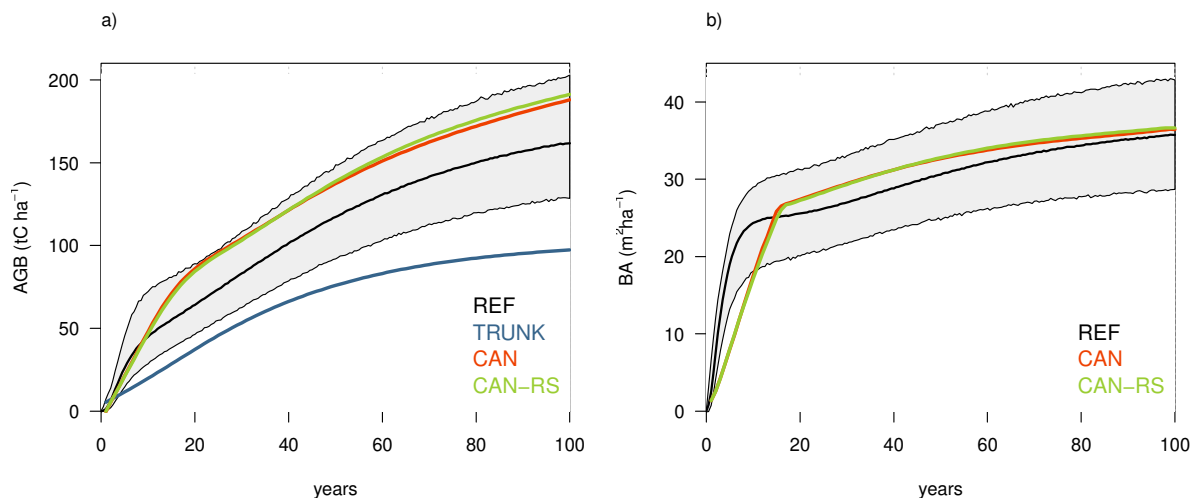

505 **Figure 7. Dynamics of (a) the aboveground biomass (AGB) and (b) basal area simulated by the different versions of ORCHIDEE during the first hundred years after clear-cut,**

compared to pseudo-data (REF) for a forest site (ARBOCEL) that was clear-cut and left regenerating in French Guiana (Chave et al., 2020).

510 In CAN-RS and CAN, the representation of stand dynamics is much more realistic than in TRUNK where woody biomass is considered to be a single pool. CAN and CAN-RS model versions allow evaluating the model for stand density and height, whereas TRUNK only produces biomass. CAN and CAN-RS have nevertheless approximations because they consider only 20 classes of tree diameter and mono-specific vegetation parameters for all trees

515 within a stand. When comparing the simulated and measured forest structure at GFG using a forest inventory and measured tree heights (Fig. 8), CAN-RS and CAN showed a realistic diameter-height allometric relationship (Fig. 8a) and a diameter-size distribution with many small trees, and few large trees (Fig. 8b). We also found that CAN-RS underestimated medium size trees with DBH ranging from 10 to 50 cm but overestimated the size of large

520 trees with DBH above 60cm (not clearly visible in Fig 8b but shown Fig. S4).
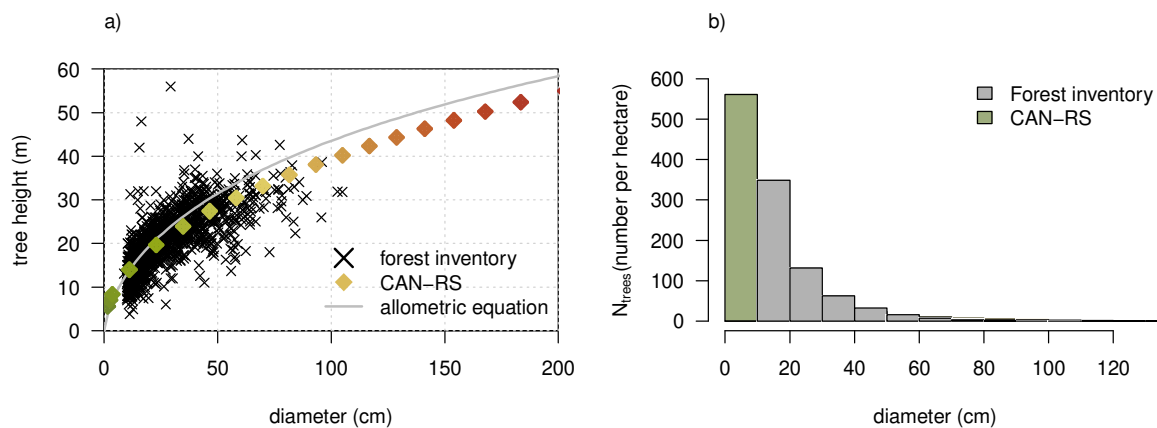
Figure 8. Forest structure modelled in CAN-RS compared to forest inventory data over non-disturbed plots at GFG (Paracou, French Guiana), with (a) allometric relationship between tree diameter and tree height for the 20 simulated diameter classes in CAN-RS

525 **plotted in colours compared to 1592 measurements; plotted in grey, the diameter-height allometric equation for tropical forest proposed by *Chave et al.*, [2014]; Eq. (6a); (b) mean diameter distribution per hectare for CAN-RS compared to data from a forest inventory of 6.25 ha plot in Paracou, French Guiana.**

530 CAN simulates a higher number of trees than observed in the Paracou inventory (930 vs 800 trees ha^{-1}), but with a smaller mean diameter (Fig. 9a). Higher GPP in CAN-RS than in CAN (especially during the dry season; Fig. 4) results into larger large trees in CAN-RS (Fig. 9a), leading to a higher self-thinning effect, and slightly fewer saplings than in CAN (Fig. 9b). This difference in forest structure translates into a higher AGB than in CAN (228 versus 206

535 tC ha^{-1}, Table 2).
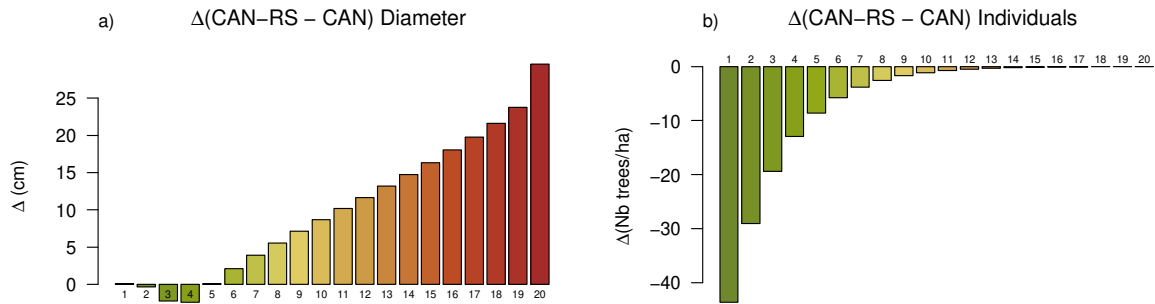
Figure 9. Comparison of the difference (Δ) between CAN-RS and CAN for: (a) mean tree diameter per cohort , here numbered from 1 to 20 and colored from green to red, and (b) the number of trees per diameter class at the GFG site (Paracou, French Guiana).

3.2 Regional evaluation

3.2.1 Carbon and water fluxes

TRUNK and CAN-RS simulation of averaged transpiration over the basin is 3.2 mm d^{-1} and match the FLUXCOM product (3.2 mm d^{-1}) (Fig. S5). While this result is encouraging, it is important to note that large uncertainties exist in gridded evapotranspiration data, and the GLEAM product indicates an ET of 2.4 mm d^{-1}). CAN-RS better captured the GPP (8 gC m^2 d^{-1}) than TRUNK (9.1 gC m^2 d^{-1}) when compared to the FLUXCOM GPP product (7.2 gC m^2 d^{-1}) (Figs. S6 and S7).

ET simulated by CAN-RS better reproduced the spatial pattern from GLEAM than TRUNK, as indicated by an increase of the Pearson spatial correlation increasing from 0.74 to 0.82. GPP simulated by CAN-RS also better reproduced the spatial pattern from FLUXCOM data than TRUNK, as indicated by an increase of the Pearson spatial correlation from 0.69 to 0.88. CAN-RS represents higher annual fluxes in the northeast and southwest of Amazonia, and lower GPP along the southeast limit of the forest (Figs. S6 and S7) that are in better agreements with the observations than TRUNK. In CAN-RS, regional maxima of ET and GPP were mainly driven by relatively high downwelling shortwave radiation, and higher precipitation (Fig. S10). TRUNK simulated a more homogeneous pattern and was less sensitive to climate gradients of the input forcing data than CAN-RS.

CAN-RS simulated higher annual mean ET and GPP than CAN over the Guiana and Brazilian Shields (the regions shown in Fig. 2) as shown in Fig. 10a and Fig. 11a. Comparison of monthly time series averaged across those two regions (Figs. 10a and 11a) shows that CAN-RS is closer to reality than CAN for both ET (R^2 = 0.81 versus 0.21 in the Guiana Shield, and 0.52 versus 0.40 in the Brazilian Shield) and GPP (R^2 = 0.42 versus 0.32 in the Guiana Shield, and 0.73 versus 0.67 in the Brazilian Shield). Indeed, CAN simulates a drastic reduction in LE and GPP during dry seasons (indicated in Fig. S11) compared to regional benchmarks (Figs. 10b-c, Figs. 11b-c). We also found that CAN-RS has a tighter relationship between

17

GPP and soil water moisture than CAN for which, in the range 700 to 1300 kg m^{-3} of soil water, GPP is nearly independent of soil moisture (Fig. S8).
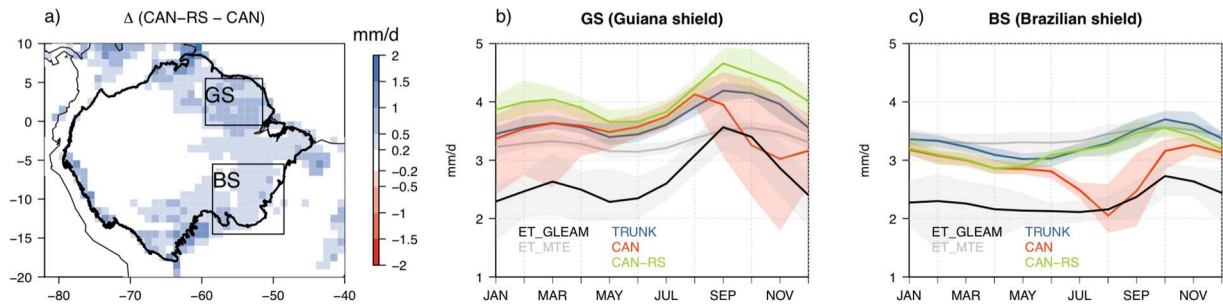
575

Figure 10. (a) Difference in annual mean evapotranspiration (ET) between the simulations of CAN-RS and CAN from 1982 to 2016. (b) Comparison of the three model versions with GLEAM and FLUXCOM (MTE) for evapotranspiration over the Guiana Shield (GS) region, and (c) same for the Brazilian Shield (BS) region. All pixels with at least 50% cover of evergreen tropical forest were included for the comparison. The shaded areas represent monthly minimum and maximum values over the entire period of simulation.
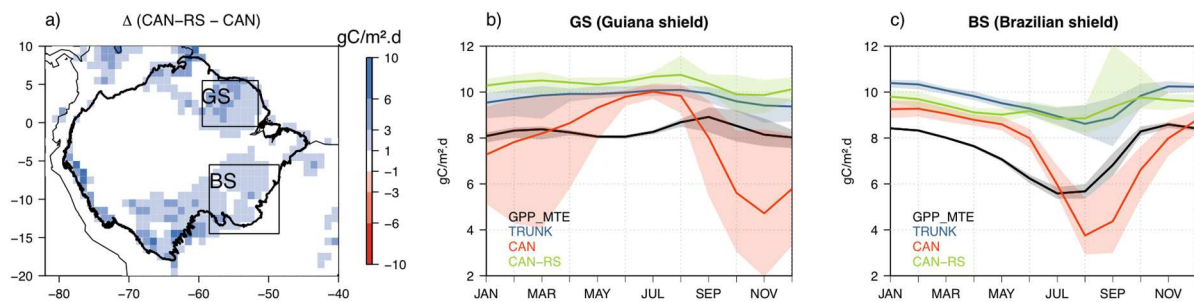

585   **Figure 11. Same than Fig. 10 but for modeled GPP compared to FLUXCOM (MTE).**

3.2.2 Carbon stocks

590   AGB stocks simulated by TRUNK were only half of those simulated by CAN-RS (Fig. S9a and b) over the Amazon. CAN-RS predicted a higher AGB than CAN over the Guiana and Brazilian shields regions (Fig. S9c), due a higher GPP during the dry seasons (Fig. 11). CAN-RS overestimated AGB, in the southwest part of the basin, which may reflect the fact that the model was calibrated using forest inventory data from sites with relatively high AGB in the
595   northeast of Amazonia (Table 1, Fig. 2 and Fig. 12). The three model versions appear to lack mechanisms controlling the observed increasing SW-NE gradient in AGB (Fig. 12). The differences between TRUNK and CAN-RS are explained by differences in both woody NPP and tree mortality. Regarding NPP, in Amazonia, the simulated carbon-use efficiency (CUE) defined by the ratio of NPP to GPP was higher in CAN-RS (0.42) than in TRUNK (0.30),
600   because of a lower maintenance respiration ($R_{A,m}$) in CAN-RS (3.1 versus 5.3 gC m^2 d^{-1}) whereas the growth respiration was slightly higher (1.4 versus 1.1 gC m^2 d^{-1}) in CAN-RS. Results from both models for CUE are in the range of field observations ranging between

18

from 0.27 to 0.52 [*Malhi et al.*, 2009a, 2015]. In CAN-RS and CAN, $R_{A,m}$ is calculated for each living compartment as a function of temperature, biomass, prescribed carbon/nitrogen
605 ratio and k_{cmaint}, the fraction of photosynthates consumed for maintenance and growth respiration (see Table S2). The parameter k_{cmaint} is poorly constrained by observations [*Sitch et al.*, 2003], and it can be optimized (e.g., as by Naudts et al. (2015)) for each site or adjusted as in this study. Thus, one of the reasons of the low AGB in TRUNK could be its low CUE (Table 1, Fig. S3 and S9). Regarding mortality, contrary to CAN in which mortality is an
610 emerging result of modelled competition processes via self-thinning (Fig. 1), in TRUNK, mortality is a constant fraction of the woody carbon pool, defined by a "residence time" parameter [*Sitch et al.*, 2003]. Thus, it is possible to capture a realistic AGB with TRUNK by adjusting this residence time value, while in CAN-RS and CAN tuning the model to reproduce AGB is less trivial.
615
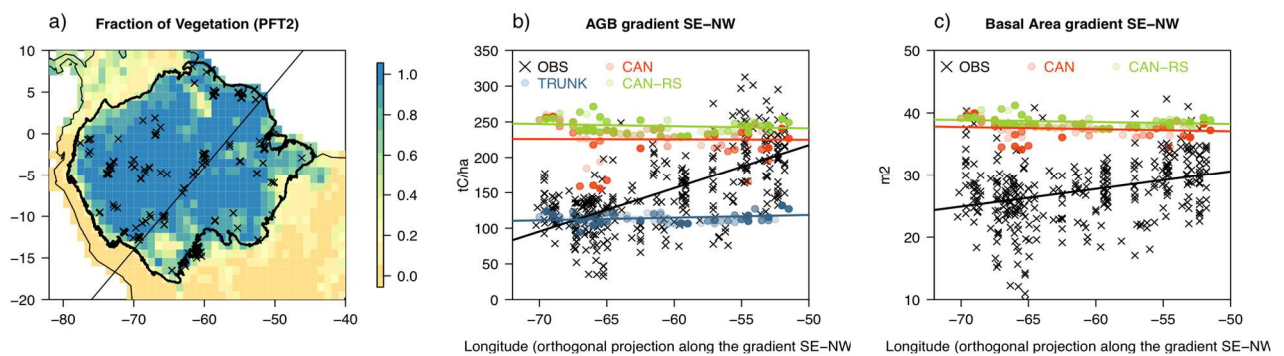
Figure 12. (a) Fraction of evergreen tropical forests (PFT2) in the model and location of the in situ inventories plots collected by *Mitchard et al.*, [2014]; (b) comparison of simulated and observed aboveground biomass (AGB) and (c) basal area.

620
4. Discussion

4.1 Root water uptake module and soil hydraulic parameters

625 In this study, we implemented a mechanistic root water uptake module that accounts for the soil-to-root resistance and its variation with soil depth and across season in the DGVM ORCHIDEE (CAN-RS). We hypothesized that a dynamic representation of plant water uptake would allow a better representation of the flux seasonality across the Amazon forest. In particular, previous models didn't simulate the sustained, or even increased, fluxes during
630 the dry season in some part of the basin by overestimating the dry season water stress (Restrepo-Coupe et al. 2017). With the root water uptake module implemented in CAN-RS, simulated tree water uptake shifts from the drier superficial top soil layers to the wetter deeper soil layers during the dry season. Through this process, the model better captured the seasonality of GPP and LE than in CAN. The effect was strongest for sites with a constraining
635 soil water retention curve, like for the clay-dominated USDA soil type 12 of our French Guiana site (GFG). A similar root water uptake model was successfully validated within another ecosystem model under severe drought conditions in Amazonia [*Fisher et al.*, 2006] and for other ecosystems by *Williams et al.* (2001), and appears to be more appropriate to

simulate transpiration during the dry season that the standard formulation based on a root biomass-weighted soil water potential. The latter indeed imposes a constant water uptake profile through seasons and years, with stronger water uptake in top soil layers that present larger root biomass. CAN-RS and TRUNK show similar performances. However, TRUNK uses an empirically calibrated formulation of soil water stress on stomatal conductance through Vcmax (see section D in SI), while in CAN-RS water supply is calculated via a more realistic hydraulic architecture inspired from *Hickler et al.* (2006). Having a mechanistic representation of soil water stress is crucial for DGVMs to understand the vegetation response to drought. Because of its mechanistic approach CAN-RS has more potential to simulate forest dynamics and fluxes under extreme conditions such as droughts.

Previous studies using land surface models with a bucket soil hydrology model and a root biomass-weighted water stress obtained a better seasonal variation of fluxes in Amazonia by setting the soil depth to 10 meters, suggesting the importance of such deep roots to sustain dry-season fluxes [*Poulter et al.*, 2009; *Verbeeck et al.*, 2011]. Evidence for such deep roots over the Amazon basin is however really scarce [*Nepstad et al.*, 1994; *Fan et al.*, 2017]. Such a setting may actually compensate for a bias in model structure due to the lack of an explicit dynamic root water uptake module, as here implemented in CAN-RS with a 4-meter soil depth. Increasing soil depth in TRUNK will always increase the water storage capacity, but it will not shift tree water uptake to the deepest layers during dry seasons since the root biomass profile is fixed to exponentially decrease from top to bottom in the soil column. With a root uptake module and a 4-meter soil depth that contains most of the fine roots (as observed by *Markewitz et al.* (2010); *Nepstad et al.* (1994); *Schenk and Jackson* (2005)), CAN-RS sustains transpiration and GPP by a shift of water uptake to deeper and wetter soil layers during the dry season, which is consistent with observations [*Moreira et al.*, 2000]. Root depth is poorly documented, as in situ investigations are highly destructive and labour intensive, and as result a great part of our knowledge derives from modelling approach [*Kleidon and Heimann*, 1998; *Ichii et al.*, 2007]. Our results suggest that model structure may have a profound effect on these model-derived estimations, and great care should be taken to avoid equifinality issues [*Medlyn et al.*, 2005].

Because they represent an explicit hydraulic architecture CAN-RS and CAN are more sensitive than TRUNK to the parameters of the Mualem-van Genuchten Model for simulating soil water stress on transpiration [*Mualem*, 1976; *van Genuchten*, 1980]. They produce a midday depression of GPP which is not observed during the dry season months (Fig. 5), suggesting an over-sensitivity to soil moisture deficits when the demand is the largest (e.g. overestimated stomatal closure or lack of tree water capacitance). It is also well known that changes in the spatial resolution of the soil input data by aggregating small-scale information causes bias in models [*Van Looy et al.*, 2017], as well as the use of a simplified classification of soil texture into few classes [*Kishné et al.*, 2017]. Thus, along with improving model representation of the hydraulic gradient from the soil to the plant in DGVMs [this study, *Sperry et al.*, 2002; *Fisher et al.*, 2006], it is important to improve the parameterization of the soil , including hydraulic parameters [*Marthews et al.*, 2014] and groundwater access.

4.2 Modeling forest structure and demography

685 As for most land surface models [*Castanho et al.*, 2015; *Johnson et al.*, 2016], the three versions of ORCHIDEE did not capture the observed increasing SW-NE gradient of AGB and BA across Amazonia (Fig. 12). The models simulate a flat AGB across the basin (Fig. S7). The observed AGB gradient can be attributed either to productivity or tree mortality, or a combination of both [*Johnson et al.*, 2016]. Spatial variation in wood productivity were

690 empirically linked to spatial variability in soil properties [*Quesada et al.*, 2012], like soil fertility [*ter Steege et al.*, 2006 ; *Malhi et al.*, 2004, *Turner et al.*, 2018] and soil hydraulic parameters. Therefore, the incorporation of detailed soil hydraulic parameters maps e.g., [*Marthews et al.*, 2014] and of nutrient cycles into ORCHIDEE should improves the simulation of the productivity gradient compared to measured observations. Besides, a

695 negative relationship was observed between soil fertility and wood density [*Baker et al.*, 2004; *ter Steege et al.*, 2006; *Patiño et al.*, 2009]. Wood density is variable across the Amazon basin, unlike being fixed like in ORCHIDEE, that could thus be improved by prescribing observed wood density maps [*ter Steege et al.*, 2006].

700 Besides variation in productivity, tree mortality has been identified as a key driver of AGB across Amazonia [*Johnson et al.*, 2016 and references within], although the processes controlling mortality variations are poorly known, and may reflect complex interactions between evolutionary selection of phenotypes and species leading to 'grow fast, die fast' emerging forest properties, with regional differences in disturbance regimes, and soil

705 hydraulic properties and fertility *[Phillips et al., 2004]* . We found that the three versions of ORCHIDEE used in this study produce a quasi-linear positive relationship between NPP and AGB, despite their differences in the representation of forest NPP and mortality (Fig. 13a). Linear emerging relationships between AGB and NPP were also found for different regions of the Amazon (Figs. S12 and S13), contrarily as showed by the observations (Johnson et al.,

710 2016). For increasing precipitation, CAN-RS and CAN showed a sharp increase in AGB followed by a saturation   at around 250 tC ha^{-1} (Fig. 13a) when precipitation is larger than 2000 mm yr^{-1} (Fig. 13b). A similar behavior was also identified by *Ahlström et al.*, [2017] over the Amazon using biomass estimated from vegetation optical depth [*Liu et al.*, 2011], which was attributed to a shift between water and radiation limited regimes, but it was not as

715 pronounced as simulated with CAN. This result suggests that when precipitation exceeds a threshold, water limitations are completely alleviated and biomass becomes controlled by other factors.

Overall, our results indicate that AGB in CAN-RS is at the upper range of observed values

720 and in the lower range for the TRUNK. An over-estimation of AGB is more 'realistic' because the three model versions do not include tropical forest disturbances (windstorms, droughts) and nutrient limitations which cause lower AGB. If these processes were to be added in TRUNK, AGB would become even lower and fall outside of the observed range. Matching biomass observations in a model like TRUNK with a well-mixed woody pool

725 formulation is very simple, and can be achieved by adjusting the constant mortality parameter. This could however lead to compensate for structural model errors such as non-

represented stand demography, and does not ensure trust in historical analysis and future projections of biomass. On the other hand, the representation of demography in a land surface model like CAN-RS is a step forward as it allows the model to be evaluated against observed
730 AGB and AGB trends while being additionally constrained by observed basal area and stand density (e.g. *Joetzjer et al.*, [2017]).

Nevertheless, since demography parameters in CAN-RS are set constant for a single PFT describing all evergreen tropical forests, spatial variability of AGB, mortality and basal area
735 (Fig. 12, 13, S13) across the Amazon remains rather uniform compared to observations, and are very comparable to the "big-leaf" version (TRUNK). Additional processes such as climate driven mortality and nutrient (phosphorus) limitation on growth leading to the prevalence of species with different functional traits across the Amazon would need to be included in the future development of this model. Besides adding PFTs, the ultimate challenge is to simulate
740 the co-existence of several PFTs over a grid cell to take into account species' diversity for above (via light) and below (water and nutrient access) ground species competition with different structures and traits (Fisher et al., 2018).
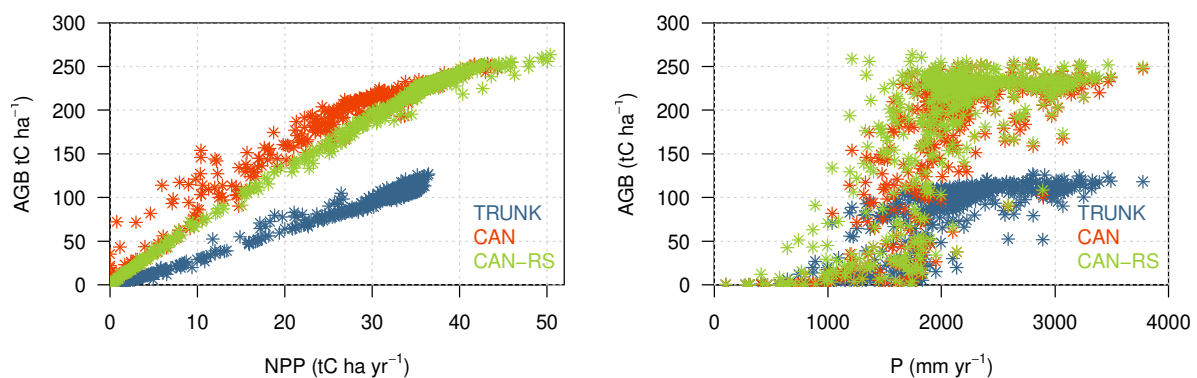
745

Figure 13. (Left) scatter plots of mean AGB from 1981 to 2016 plotted against mean annual NPP and (Right) annual precipitation averaged over the same time period for Amazonia.

750 **4.3 Conclusion**

The new description of tropical forest demography in CAN-RS (and CAN) presented in this study allows to simulate observable stand structure variables (diameter and height distributions, and stand density) and go beyond the simulation paradigm of treating biomass
755 as a single carbon pool with a constant mortality rate, as done in many global land surface models, including the TRUNK version of ORCHIDEE. Including recruitment, differentiated diameter classes growth rates and density dependent mortality allows to evaluate tree mortality and stand level growth using forest inventory data. Overall, CAN-RS reasonably simulates in-situ forest's structure. On the whole, CAN-RS better captures ET and GPP

annual mean fluxes at 2 sites, reduces the positive bias in GPP at regional scale and improves the spatial representation of GPP and ET when compared to the TRUNK. Nevertheless, additional processes such as climate driven mortality and nutrient (phosphorus) limitation on growth leading to the prevalence of species with different functional traits across the Amazon would need to be included in the future development of this model. We can note that CAN-RS tends to over-estimate regional AGB stocks observations, since the model lacks mortality processes induced by drought and other disturbances. The new formulation of soil water uptake by deep-rooted trees implemented in CAN-RS indicates that the hypothesis of preferential soil water use better matches the data than the hypothesis of root-biomass-driven water uptake (in CAN), meaning that trees preferentially use water in the deepest soil layer during the dry season which led to improve the seasonality of evapotranspiration and canopy photosynthesis, especially for clay soils for which the soil moisture potential drops rapidly when soil moisture decreases in the dry season.

References

Ahlström, A., J. G. Canadell, G. Schurgers, M. Wu, J. A. Berry, K. Guan, and R. B. Jackson (2017), Hydrologic resilience and Amazon productivity, *Nat. Commun.*, *8*(1), 1–9, doi:10.1038/s41467-017-00306-z.

Arora, V. K. et al. (2013), Carbon–Concentration and Carbon–Climate Feedbacks in CMIP5 Earth System Models, *J. Clim.*, *26*(15), 5289–5314, doi:10.1175/JCLI-D-12-00494.1.

Baker, T. et al. (2004), Increasing biomass in Amazonian forest plots, *Philos. Trans. R. Soc. Lond. B. Biol. Sci.*, doi:10.1098/rstb.2003.1422.

Bellassen, V., G. Le Maire, DhôteJ.F., P. Ciais, and N. Viovy (2010), Modelling forest management within a global vegetation model-Part 1: Model structure and general behaviour, *Ecol. Modell.*, *221*(20), 2458–2474, doi:10.1016/j.ecolmodel.2010.07.008.

Bellassen, V., G. le Maire, O. Guin, J. F. Dhôte, P. Ciais, and N. Viovy (2011), Modelling forest management within a global vegetation model-Part 2: Model validation from a tree to a continental scale, *Ecol. Modell.*, *222*(1), 57–75, doi:10.1016/j.ecolmodel.2010.08.038.

Bonal, D. et al. (2008), Impact of severe dry season on net ecosystem exchange in the Neotropical rainforest of French Guiana, *Glob. Chang. Biol.*, *14*(8), 1917–1933, doi:10.1111/j.1365-2486.2008.01610.x.

Bonan, G. B., M. Williams, R. a. Fisher, and K. W. Oleson (2014), Modeling stomatal conductance in the earth system: linking leaf water-use efficiency and water transport along the soil–plant–atmosphere continuum, *Geosci. Model Dev.*, *7*(5), 2193–2222, doi:10.5194/gmd-7-2193-2014.

Booth, B. B. B., C. D. Jones, M. Collins, I. J. Totterdell, P. M. Cox, S. Sitch, C. Huntingford,

R. a Betts, G. R. Harris, and J. Lloyd (2012), High sensitivity of future global warming to land carbon cycle processes, *Environ. Res. Lett.*, *7*(2), 024002, doi:10.1088/1748-9326/7/2/024002.

810 Brienen, R. J. W. et al. (2015), Long-term decline of the Amazon carbon sink, *Nature*, *519*(7543), 344–348, doi:10.1038/nature14283.

Campoy, A., A. Ducharne, F. Cheruy, F. Hourdin, J. Polcher, and J. C. Dupont (2013), Response of land surface fluxes and precipitation to different soil bottom hydrological conditions in a general circulation model, *J. Geophys. Res. Atmos.*, *118*(19), 10725–

815 10739, doi:10.1002/jgrd.50627.

Carsel, R. F., and R. S. Parrish (1988), Developing joint probability distributions of soil water retention characteristics, *Water Resour. Res.*, *24*(5), 755–769, doi:10.1029/WR024i005p00755.

Castanho, A. D. A., D. Galbraith, K. Zhang, M. T. Coe, M. H. Costa, and P. Moorcroft

820 (2015), Changing Amazon biomass and the role of atmospheric CO2 concentration, climate, and land use, *Global Biogeochem. Cycles*, *30*, 18–39, doi:10.1002/2015GB005135.Received.

Chave, J. et al. (2005), Tree allometry and improved estimation of carbon stocks and balance in tropical forests., *Oecologia*, *145*(1), 87–99, doi:10.1007/s00442-005-0100-x.

825 Chave, J. et al. (2014), Improved allometric models to estimate the aboveground biomass of tropical trees, *Glob. Chang. Biol.*, *20*(10), 3177–3190, doi:10.1111/gcb.12629.

Chave, J., et al. (2020). Slow rate of secondary forest carbon accumulation in the Guianas compared with the rest of the Neotropics. *Ecological Applications, 30*(1), e02004.

Christoffersen, B. O. et al. (2014), Mechanisms of water supply and vegetation demand

830 govern the seasonality and magnitude of evapotranspiration in Amazonia and Cerrado, *Agric. For. Meteorol.*, *191*(February), 33–50, doi:10.1016/j.agrformet.2014.02.008.

Christoffersen, B. O. et al. (2016), Linking hydraulic traits to tropical forest function in a size-structured and trait-driven model (TFS v.1-Hydro), *Geosci. Model Dev. Discuss.*, *0*(June), 1–60, doi:10.5194/gmd-2016-128.

835

Denslow, J. S., Ellison, A. M., & Sanford, R. E. (1998). Treefall gap size effects on above-and below-ground processes in a tropical wet forest. *Journal of Ecology, 86*(4), 597-609.

Deleuze, C., O. Pain, J. Dhote, and J.-C. Hervé (2004), A flexible radial increment model for

840 individual trees in pure age stands, *Ann. For. Sci.*, *61*(4), 327–335, doi:10.1051/forest.

Dubois-Fernandez, P. C., T. Le Toan, S. Daniel, H. Oriot, J. Chave, L. Blanc, L. Villard, M. W. J. Davidson, and M. Petit (2012), The tropiSAR airborne campaign in French Guiana: Objectives, description, and observed temporal behavior of the backscatter signal, *IEEE Trans. Geosci. Remote Sens.*, *50*(8), 3228–3241,

845 doi:10.1109/TGRS.2011.2180728.

Duursma, R. A., and B. E. Medlyn (2012), MAESPA: A model to study interactions between water limitation, environmental drivers and vegetation function at tree and stand levels, with an example application to CO2 drought interactions, *Geosci. Model Dev.*, *5*(4), 919–940, doi:10.5194/gmd-5-919-2012.

850 Eltahir, E. a. B., and R. L. Bras (1994), Precipitation recycling in the Amazon basin, *Q. J. R. Meteorol. Soc.*, *120*(518), 861–880, doi:10.1002/qj.49712051806.

Fan, Y., G. Miguez-Macho, E. G. Jobbágy, R. B. Jackson, and C. Otero-Casal (2017), Hydrologic regulation of plant rooting depth, *Proc. Natl. Acad. Sci. U. S. A.*, *114*(40), 10572–10577, doi:10.1073/pnas.1712381114.

855 Farquhar, G., S. von Caemmerer, and J. Berry (1980), A biochemical model of photosynthetic CO2 assimilation in leaves of C3 species, *Planta*, *90*, 78–90.

Farrior, C. E., S. A. Bohlman, S. Hubbell, and S. W. Pacala (2016), Dominance of the

suppressed: Power-law size structure in tropical forests, , *351*(6269), 2014–2016, doi:10.1126/science.aad0592.

860   Fisher, R., N. McDowell, D. Purves, P. Moorcroft, S. Sitch, P. Cox, C. Huntingford, P. Meir, and F. I. Woodward (2010), Assessing uncertainties in a second-generation dynamic vegetation model caused by ecological scale limitations., *New Phytol.*, *187*(3), 666–81, doi:10.1111/j.1469-8137.2010.03340.x.

Fisher, R. A. et al. (2018), Vegetation demographics in Earth System Models: A review of
865   progress and priorities, *Glob. Chang. Biol.*, *24*(1), 35–54, doi:10.1111/gcb.13910.

Fisher, R. a, M. Williams, R. L. Do Vale, A. L. Da Costa, and P. Meir (2006), Evidence from Amazonian forests is consistent with isohydric control of leaf water potential., *Plant. Cell Environ.*, *29*(2), 151–65.

Gardner, W. R. (1960), Dynamic aspects of water availability to plants, *Soil Sci.*, *89*(2), 63–
870   73, doi:10.1097/00010694-196002000-00001.

van Genuchten, M. T. (1980), A Closed-form Equation for Predicting the Hydraulic Conductivity of Unsaturated Soils1, *Soil Sci. Soc. Am. J.*, *44*(5), 892, doi:10.2136/sssaj1980.03615995004400050002x.

Getirana, A. C. V. et al. (2014), Water Balance in the Amazon Basin from a Land Surface
875   Model Ensemble, *J. Hydrometeorol.*, *15*(6), 2586–2614, doi:10.1175/JHM-D-14-0068.1.

Gourlet-Fleury, S., B. Ferry, J.-F. Molino, P. Petronelli, and L. Schmitt (2004), Paracou expérimental plots : keys features, in *Ecology and management of a neotropical rainforest : lessons drawn from Paracou, a long-term experimental research site in French Guiana*, pp. 3–60.

880   Guimberteau, M., P. Ciais, A. Ducharne, J. P. Boisier, S. Peng, M. De Weirdt, and H. Verbeeck (2014), Two soil hydrology formulations of ORCHIDEE (version Trunk.rev1311) tested for the Amazon basin, *Geosci. Model Dev.*, *7*(1), 73–129, doi:10.5194/gmdd-7-73-2014.

Haverd, V., J. L. Lovell, M. Cuntz, D. L. B. Jupp, G. J. Newnham, and W. Sea (2012), The
885   Canopy Semi-analytic P gap And Radiative Transfer (CanSPART) model: Formulation and application, *Agric. For. Meteorol.*, *160*, 14–35, doi:10.1016/j.agrformet.2012.01.018.

Hickler, T., I. C. Prentice, B. Smith, M. T. Sykes, and S. Zaehle (2006), Implementing plant hydraulic architecture within the LPJ Dynamic Global Vegetation Model, *Glob. Ecol.*
890   *Biogeogr.*, *15*(6), 567–577, doi:10.1111/j.1466-8238.2006.00254.x.

Ho Tong Minh, D. et al. (2016), SAR tomography for the retrieval of forest biomass and height: Cross-validation at two tropical forest sites in French Guiana, *Remote Sens. Environ.*, *175*, 138–147, doi:10.1016/j.rse.2015.12.037.

Hollinger, D. Y., and A. D. Richardson (2005), Uncertainty in eddy covariance measurements
895   and its application to physiological models., *Tree Physiol.*, *25*(7), 873–85.

Ichii, K., H. Hashimoto, M. A. White, C. Potter, L. R. Hutyra, A. R. Huete, R. B. Myneni, and R. R. Nemani (2007), Constraining rooting depths in tropical rainforests using satellite data and ecosystem modeling for accurate simulation of gross primary production seasonality, *Glob. Chang. Biol.*, *13*(1), 67–77, doi:10.1111/j.1365-2486.2006.01277.x.

900   Joetzjer, E. et al. (2014), Predicting the response of the Amazon rainforest to persistent drought conditions under current and future climates: a major challenge for global land surface models, *Geosci. Model Dev.*, *7*(6), 2933–2950, doi:10.5194/gmd-7-2933-2014.

Joetzjer, E. et al. (2017), Assimilating satellite-based canopy height within an ecosystem model to estimate above ground forest biomass, *Geophys. Res. Lett.*, 1–10,
905   doi:10.1002/2017GL074150.

Johnson, M. O. et al. (2016), Variation in stem mortality rates determines patterns of above-ground biomass in Amazonian forests: implications for dynamic global vegetation

models, *Glob. Chang. Biol.*, *22*(12), 3996–4013, doi:10.1111/gcb.13315.

Jones, C. et al. (2013), Twenty-First-Century Compatible CO 2 Emissions and Airborne
Fraction Simulated by CMIP5 Earth System Models under Four Representative
Concentration Pathways, *J. Clim.*, *26*(13), 4398–4413, doi:10.1175/JCLI-D-12-00554.1.

Jung, M. et al. (2011), Global patterns of land-atmosphere fluxes of carbon dioxide, latent
heat, and sensible heat derived from eddy covariance, satellite, and meteorological
observations, *J. Geophys. Res.*, *116*, 1–16, doi:10.1029/2010JG001566.

Jung, M. et al. (2017), Compensatory water effects link yearly global land CO 2 sink changes
to temperature, *Nature*, *541*(7638), 516–520, doi:10.1038/nature20780.

Kennedy, D., R. A. Fisher, S. Swenson, and K. W. Oleson (2019), Implementing plant
hydraulics in the Community Land Model, version 5, *J. Adv. Model. Earth Syst.*,
doi:10.1029/2018ms001500.

Kishné, A. S., Y. T. Yimam, C. L. S. Morgan, and B. C. Dornblaser (2017), Evaluation and
improvement of the default soil hydraulic parameters for the Noah Land Surface Model,
Geoderma, *285*, 247–259, doi:10.1016/j.geoderma.2016.09.022.

Kleidon, A., and M. Heimann (1998), A method of determining rooting depth from a
terrestrial biosphere model and its impacts on the global water and carbon cycle, *Glob.
Chang. Biol.*, *4*(3), 275–286, doi:10.1046/j.1365-2486.1998.00152.x.

Kohyama, T. (1992), Density-size dynamics of trees simulated by a one-sided competition
multi-species model of rain forest stands, *Ann. Bot.*, *70*(5), 451–460,
doi:10.1093/oxfordjournals.aob.a088502.

Krinner, G., N. Viovy, N. de Noblet-Ducoudré, J. Ogée, J. Polcher, P. Friedlingstein, P. Ciais,
S. Sitch, and I. C. Prentice (2005), A dynamic global vegetation model for studies of the
coupled atmosphere-biosphere system, *Global Biogeochem. Cycles*, *19*(1),
doi:10.1029/2003GB002199.

Larcher, W. (2003), The environment of plantst, in *Physiological Plant Ecology*, pp. 1–67.

Lardy, R., G. Bellocchi, and J. F. Soussana (2011), A new method to determine soil organic
carbon equilibrium, *Environ. Model. Softw.*, *26*(12), 1759–1763,
doi:10.1016/j.envsoft.2011.05.016.

Lasslop, G., M. Reichstein, D. Papale, A. D. Richardson, A. Arneth, A. Barr, P. Stoy, and G.
Wohlfahrt (2010), Separation of net ecosystem exchange into assimilation and
respiration using a light response curve approach: critical issues and global evaluation,
Glob. Chang. Biol., *16*(1), 187–208, doi:10.1111/j.1365-2486.2009.02041.x.

Levine, N. M. et al. (2016), Ecosystem heterogeneity determines the ecological resilience of
the Amazon to climate change., *Proc. Natl. Acad. Sci. U. S. A.*, *113*(3), 1511344112-,
doi:10.1073/pnas.1511344112.

Liu, Y. Y., R. A. M. De Jeu, M. F. McCabe, J. P. Evans, and A. I. J. M. Van Dijk (2011),
Global long-term passive microwave satellite-based retrievals of vegetation optical
depth, *Geophys. Res. Lett.*, *38*(18), 1–6, doi:10.1029/2011GL048684.

Longo, M. et al. (2018), Ecosystem heterogeneity and diversity mitigate Amazon forest
resilience to frequent extreme droughts, *New Phytol.*, *219*(3), 914–931,
doi:10.1111/nph.15185.

Van Looy, K. et al. (2017), Pedotransfer Functions in Earth System Science: Challenges and
Perspectives, *Rev. Geophys.*, *55*(4), 1199–1256, doi:10.1002/2017RG000581.

Lovenduski, N. S., and G. B. Bonan (2017), Reducing uncertainty in projections of terrestrial
carbon uptake, , *12*, doi:10.1088/1748-9326/aa66b8.

Maeda, E. E., Ma, X., Wagner, F. H., Kim, H., Oki, T., Eamus, D., & Huete, A. (2017).
Evapotranspiration seasonality across the Amazon Basin. *Earth System Dynamics*, *8*(2), 439-454.

Malhi, Y. et al. (2009a), Comprehensive assessment of carbon productivity, allocation and

storage in three Amazonian forests, *Glob. Chang. Biol.*, *15*(5), 1255–1274,
doi:10.1111/j.1365-2486.2008.01780.x.

Malhi, Y., S. Saatchi, C. Girardin, and L. Aragão (2009b), The production, storage, and flow of carbon in Amazonian forests, *Geophys. Monogr. Ser.*, 355–372.

Malhi, Y. et al. (2015), The linkages between photosynthesis, productivity, growth and biomass in lowland Amazonian forests, *Glob. Chang. Biol.*, *21*(6), 2283–2295, doi:10.1111/gcb.12859.

Maréchaux, I., and J. Chave (2017), An individual-based forest model to jointly simulate carbon and tree diversity in Amazonia: description and applications, *Ecol. Monogr.*, *0*(0), 1–33, doi:10.1002/ecm.1271.

Markewitz, D., S. Devine, E. a Davidson, P. Brando, and D. C. Nepstad (2010), Soil moisture depletion under simulated drought in the Amazon: impacts on deep root uptake., *New Phytol.*, *187*(3), 592–607, doi:10.1111/j.1469-8137.2010.03391.x.

Martens, B., D. G. Miralles, H. Lievens, R. Van Der Schalie, R. A. M. De Jeu, D. Fernández-Prieto, H. E. Beck, W. A. Dorigo, and N. E. C. Verhoest (2017), GLEAM v3: Satellite-based land evaporation and root-zone soil moisture, *Geosci. Model Dev.*, *10*(5), 1903–1925, doi:10.5194/gmd-10-1903-2017.

Marthews, T. R., C. A. Quesada, D. R. Galbraith, Y. Malhi, C. E. Mullins, M. G. Hodnett, and I. Dharssi (2014), High-resolution hydraulic parameter maps for surface soils in tropical South America, *Geosci. Model Dev.*, *7*(3), 711–723, doi:10.5194/gmd-7-711-2014.

McGrath, M. J., J. Ryder, B. Pinty, J. Otto, K. Naudts, A. Valade, Y. Chen, J. Weedon, and S. Luyssaert (2016), A multi-level canopy radiative transfer scheme for ORCHIDEE (SVN~r2566), based on a domain-averaged structure factor, *Geosci. Model Dev. Discuss.*, *2016*(November), 1–22, doi:10.5194/gmd-2016-280.

Medlyn, B. E., A. P. Robinson, R. Clement, and R. E. McMurtrie (2005), On the validation of models of forest CO2 exchange using eddy covariance data: Some perils and pitfalls, *Tree Physiol.*, *25*(7), 839–857, doi:10.1093/treephys/25.7.839.

Metcalfe, D. B. et al. (2008), The effects of water availability on root growth and morphology in an Amazon rainforest, *Plant Soil*, *311*(1–2), 189–199, doi:10.1007/s11104-008-9670-9.

Meyer, V., S. Saatchi, D. B. Clark, M. Keller, G. Vincent, A. Ferraz, F. Espírito-Santo, M. V. N. d&apos;Oliveira, D. Kaki, and J. Chave (2018), Canopy Area of Large Trees Explains Aboveground Biomass Variations across Nine Neotropical Forest Landscapes, *Biogeosciences Discuss.*, (January), 1–38, doi:10.5194/bg-2017-547.

Mitchard, E. T. a. et al. (2014), Markedly divergent estimates of Amazon forest carbon density from ground plots and satellites, *Glob. Ecol. Biogeogr.*, n/a-n/a, doi:10.1111/geb.12168.

Moreira, A. A., D. Santini, and A. L. Ruhoff (2018), Avaliação dos produtos de evapotranspiração baseados em sensoriamento remoto MOD16 e GLEAM em sítios de fluxos turbulentos do Programa LBA Evaluation of remotely sensed evapotranspiration products MOD16 and GLEAM in eddy covariance flux sites from LBA Pro, *Cienca e Nat.*, 112–118, doi:10.5902/2179460X30714.

Moreira, M. Z., L. D. L. Sternberg, and D. C. Nepstad (2000), Vertical patterns of soil water uptake by plants in a primary forest and an abandoned pasture in the eastern Amazon: an isotopic approach, *Plant Soil*, *222*(1–2), 95–107, doi:10.1023/A:1004773217189.

Mualem, Y. (1976), A new model for predicting the hydraulic conductivity of unsaturated porous media, *Water Resour. Res.*, *12*(3), 513–521.

Naudts, K. et al. (2015), A vertically discretised canopy description for ORCHIDEE (SVN r2290) and the modifications to the energy, water and carbon fluxes, *Geosci. Model*

Dev., *8*(6), 2035–2065, doi:10.5194/gmdd-7-8565-2014.

1010   Nepstad, D. C., C. R. de Carvalho, E. A. Davidson, P. H. Jipp, P. A. Lefebvre, G. H. Negreiros, E. D. da Silva, T. A. Stone, S. E. Trumbore, and S. Vieira (1994), The role of deep roots in the hydrological and carbon cycles of Amazonian forests and pastures, *Nature*, *372*, 666–669, doi:10.1038/372666a0.

Nepstad, D. C., I. M. Tohver, D. Ray, P. Moutinho, and G. Cardinot (2007), Mortality of

1015   large trees and lianas following experimental drought in an Amazon forest., *Ecology*, *88*(9), 2259–69.

Newman, E. I. (1969), Resistance to Water Flow in Soil and Plant . I . Soil Resistance in Relation to Amounts of Root : Theoretical Estimates Author (s): E . I . Newman Source : Journal of Applied Ecology , Vol . 6 , No . 1 (Apr ., 1969), pp . 1-12 Published

1020   by : British E, *J. Appl. Ecol.*, *6*(1), 1–12.

Paca, V. H. da M., G. E. Espinoza-Dávalos, T. M. Hessels, D. M. Moreira, G. F. Comair, and W. G. M. Bastiaanssen (2019), The spatial variability of actual evapotranspiration across the Amazon River Basin based on remote sensing products validated with flux towers, *Ecol. Process.*, *8*(1), doi:10.1186/s13717-019-0158-8.

1025   Patiño, S., J. Lloyd, and R. Paiva (2009), Branch xylem density variations across the Amazon Basin, *Biogeosciences*, (May 2008), 545–568.

Phillips, O. L. et al. (2002), Changes in growth of tropical forests: Evaluating potential biases, *Ecol. Apr 2002; 12 576-587*, *12*(2), 576–587.

Phillips, O. L., & Gentry, A. H. (1994). Increasing turnover through time in tropical

1030   forests. *Science*, *263*(5149), 954-958.

Phillips, O. L., Baker, T. R., Arroyo, L., Higuchi, N., Killeen, T. J., Laurance, W. F., ... & Vinceti, B. (2004). Pattern and process in Amazon tree turnover, 1976–2001. *Philosophical Transactions of the Royal Society of London. Series B: Biological Sciences*, *359*(1443), 381-407.

1035

Pillet, M., E. Joetzjer, C. Belmin, J. Chave, P. Ciais, A. Dourdain, M. Evans, B. Hérault, S. Luyssaert, and B. Poulter (2017), Disentangling competitive versus climatic drivers of tropical forest mortality, *J. Ecol.*, (July), 1–15, doi:10.1111/1365-2745.12876.

Poulter, B., U. Heyder, and W. Cramer (2009), Modeling the Sensitivity of the Seasonal

1040   Cycle of GPP to Dynamic LAI and Soil Depths in Tropical Rainforests, *Ecosystems*, *12*(4), 517–533, doi:10.1007/s10021-009-9238-4.

Poulter, B., L. Aragão, U. Heyder, M. Gumpenberger, J. Heinke, F. Langerwisch, A. Rammig, K. Thonicke, and W. Cramer (2010), Net biome production of the Amazon Basin in the 21st century, *Glob. Chang. Biol.*, *16*(7), 2062–2075, doi:10.1111/j.1365-

1045   2486.2009.02064.x.

Powell, T. L. et al. (2013), Confronting model predictions of carbon fluxes with measurements of Amazon forests subjected to experimental drought., *New Phytol.*, doi:10.1111/nph.12390.

Prentice, I. C., X. Liang, B. E. Medlyn, and Y. P. Wang (2015), Reliable, robust and realistic:

1050   The three R's of next-generation land-surface modelling, *Atmos. Chem. Phys.*, *15*(10), 5987–6005, doi:10.5194/acp-15-5987-2015.

Pyle, E. H. et al. (2008), Dynamics of carbon, biomass, and structure in two Amazonian forests, *J. Geophys. Res.*, *113*, doi:10.1029/2007JG000592.

Quesada, C. A., J. Lloyd, L. O. Anderson, N. M. Fyllas, M. Schwarz, and C. I. Czimczik

1055   (2011), Soils of Amazonia with particular reference to the RAINFOR sites, *Biogeosciences*, *8*(6), 1415–1440, doi:10.5194/bg-8-1415-2011.

Reichstein, M. et al. (2005), On the separation of net ecosystem exchange into assimilation and ecosystem respiration: review and improved algorithm, *Glob. Chang. Biol.*, *11*(9), 1424–1439, doi:10.1111/j.1365-2486.2005.001002.x.

1060   Reineke, L. H. (1933), Perfecting a stand-density index for even-aged forests, *J. Agric. Res.*, *46*(7), 627–638.

Restrepo-Coupe, N. et al. (2016), Do dynamic global vegetation models capture the seasonality of carbon fluxes in the Amazon basin? A data-model intercomparison, *Glob. Chang. Biol.*, 191–208, doi:10.1111/gcb.13442.

1065   Rocha, H. Da (2004), Diel and seasonal patterns of tropical forest CO_2 exchange, *Ecol. Appl.*, *14*(4), 22–32.

da Rocha, H. R. et al. (2009), Patterns of water and heat flux across a biome gradient from tropical forest to savanna in Brazil, *J. Geophys. Res.*, *114*, G00B12, doi:10.1029/2007JG000640.

1070   Rödig, E., M. Cuntz, A. Rammig, R. Fischer, F. Taubert, and A. Huth (2018), The importance of forest structure for carbon flux estimates in the Amazon rainforest, *Environ. Res. Lett.*, *in press*, doi:https://doi.org/10.1088/1748-9326/aabc61.

de Rosnay, P., and J. Polcher (1998), Modelling root water uptake in a complex land surface scheme coupled to a GCM, *Hydrol. Earth Syst. Sci.*, *2*(2/3), 239–255, doi:10.5194/hess-
1075   2-239-1998.

de Rosnay, P. De, J. Polcher, M. Bruen, and K. Laval (2002), Impact of a physically based soil water flow and soil-plant interaction representation for modeling large-scale land surface processes, , *107*(2).

Rüger, N., Huth, A., Hubbell, S. P., & Condit, R. (2009). Response of recruitment to light
1080 availability across a tropical lowland rain forest community. *Journal of Ecology*, *97*(6), 1360-1368.

Sakschewski, B., W. von Bloh, A. Boit, L. Poorter, M. Peña-Claros, J. Heinke, J. Joshi, and K. Thonicke (2016), Resilience of Amazon forests emerges from plant trait diversity,
1085   *Nat. Clim. Chang.*, *6*(11), 1032–1036, doi:10.1038/nclimate3109.

Schenk, H. J., and R. B. Jackson (2005), Mapping the global distribution of deep roots in relation to climate and soil characteristics, *Geoderma*, *126*(1–2 SPEC. ISS.), 129–140, doi:10.1016/j.geoderma.2004.11.018.

Schmidhalter, U. (1997), The gradient between pre-dawn rhizoplane and bulk soil matric
1090   potentials, and its relation to the pre-dawn root and leaf water potentials of four species, *Plant, Cell Environ.*, *20*(7), 953–960, doi:10.1046/j.1365-3040.1997.d01-136.x.

Shinozaki, K. Y. K. H. K. K. T. (1964), A quantitative analysis of plant form - the pipe model theory I. Basic analyses, *Japanese J. Ecol.*

Sitch, S., B. Smith, and I. Prentice (2003), Evaluation of ecosystem dynamics, plant
1095   geography and terrestrial carbon cycling in the LPJ dynamic global vegetation model, *Glob. Chang. Biol.*, 161–185.

Sitch, S. et al. (2015), Recent trends and drivers of regional sources and sinks of carbon dioxide, *Biogeosciences*, *12*(3), 653–679, doi:10.5194/bg-12-653-2015.

Sperry, J. S., U. G. Hacke, R. Oren, and J. P. Comstock (2002), Water deficits and hydraulic
1100   limits to leaf water supply, *Plant. Cell Environ.*, *25*(2), 251–263.

ter Steege, H. et al. (2006), Continental-scale patterns of canopy tree composition and function across Amazonia., *Nature*, *443*(7110), 0–2, doi:10.1038/nature05134.

Taylor, K. E. (2001), in a Single Diagram, *J. Geophys. Res.*, *106*(D7), 7183–7192.

Tramontana, G. et al. (2016), Predicting carbon dioxide and energy fluxes across global
1105   FLUXNET sites with regression algorithms, *Biogeosciences*, *13*(14), 4291–4313, doi:10.5194/bg-13-4291-2016.

Verbeeck, H., P. Peylin, C. Bacour, D. Bonal, K. Steppe, and P. Ciais (2011), Seasonal patterns of CO 2 fluxes in Amazon forests: Fusion of eddy covariance data and the ORCHIDEE model, *J. Geophys. Res.*, *116*(G2), 1–19, doi:10.1029/2010JG001544.

1110 Wei, Y. et al. (2014), The north american carbon program multi-scale synthesis and terrestrial model intercomparison project - Part 2: Environmental driver data, *Geosci. Model Dev.*, *7*(6), 2875–2893, doi:10.5194/gmd-7-2875-2014.

Werth, D., and R. Avissar (2002), The local and global effects of Amazon deforestation David, *Geophys. Res. Lett.*, *107*(55), 1–7, doi:10.1029/2001JD000717.

1115 Williams, M., B. J. Bond, and M. G. Ryan (2001), Evaluating different soil and plant hydraulic constraints on tree function using a model and sap flow data from ponderosa pine, *Plant, Cell Environ.*, *24*(7), 679–690, doi:10.1046/j.1365-3040.2001.00715.x.

Wilson, K. (2002), Energy balance closure at FLUXNET sites, *Agric. For. Meteorol.*, *113*(1–4), 223–243, doi:10.1016/S0168-1923(02)00109-0.

1120 Xu, X., D. Medvigy, J. S. Powers, J. M. Becknell, and K. Guan (2016), Diversity in plant hydraulic traits explains seasonal and inter-annual variations of vegetation dynamics in seasonally dry tropical ... Diversity in plant hydraulic traits explains seasonal and inter-annual variations of vegetation dynamics in seasonally, *New Phytol.*, *212*(May), 80–95, doi:10.1111/nph.14009.

1125 Yoda, K., Kira, T., Ogawa, H., and Hozumi, K.: Self-thinning in overcrowded pure stands under cultivated and natural conditions, J. Inst. Polytech. (Osaka University), 14, 107–129, 1963

Zhang, K. et al. (2015), The fate of Amazonian ecosystems over the coming century arising from changes in climate, atmospheric CO_2, and land use, *Glob. Chang. Biol.*, *21*(7),
1130 2569–2587, doi:10.1111/gcb.12903.

Code availability

1135

The code of ORCHIDEE-CAN r2290 (Naudts et al., 2015) can be accessed from http://dx.doi.org/10.14768/06337394-73A9-407C-9997-0E380DAC5595